

Recent Developments in VQE: Survey and Benchmarking

Taylor Harville, Rishu Khurana, Vitor F. Grizzi, Cong Liu*

*Chemical Sciences and Engineering Division, Argonne National Laboratory, Lemont, IL 60439,
United States*

E-mail: congliu@anl.gov

Abstract

The Variational Quantum Eigensolver (VQE) algorithm has been developed to target near term Noisy Intermediate Scale Quantum (NISQ) computers as a method to find the eigenvalues of Hamiltonians. Unlike fully quantum algorithms such as Quantum Phase Estimation (QPE), VQE based methods are hybrid algorithms that utilize both quantum and classical hardware to combat issues with the near term quantum hardware such as small numbers of available qubits and the decoherence of qubits. Different adaptations (flavors) of VQE have been implemented to combat these scalability issues on NISQ devices compared to standard VQE. These different flavors are modifications of the underlying VQE ansatz to reduce the computational workload on the quantum hardware. In this review we focus on 3 main areas related to VQE. The first focus is on flavors of VQE that fall under the categories of circuit complexity reduction, chemistry inspired ansatz, and extensions of VQE to excited states. The remaining portion of the review focuses on benchmarking the accuracy of VQE methods and an overview of the current state of quantum simulators.

1 Introduction

Use of first principles, or *ab initio*, calculations to understand properties of molecules and materials has been a staple of computational chemistry for decades. The foundation of *ab initio* calculations is to approximately solve Schrodinger's equation giving insight into the electronic structure and geometry of chemical systems. The computational cost of solving these approximate methods on a classical computer scales exponentially with relation to system size. Recent advances in high performance parallel computing, in conjunction with advanced algorithmic development to deploy the algorithms on parallel hardware, has led to an increase in the size of systems that can be studied, but the growth of classical computing hardware cannot scale fast enough to overcome the exponential scaling of quantum chemistry methods. The underlying problem was addressed by Feynman in his famous paper in 1982, "Simulating Physics with Computers" that launched the field of quantum computing.¹ Feynman's main postulate explained that in order to effectively simulate quantum systems one needed to utilize quantum hardware on some type of quantum computer. The molecular interactions chemists want to model can more easily be mapped to a quantum hardware than the classical hardware that has prevailed so far. The use of quantum computers to model systems too large or complex to be tractable on classical hardware is termed the quantum advantage. Quantum computers have many near term problems that delay the era of quantum advantage. The main limitations of current quantum hardware are the small number and decoherence of the qubits that make up the quantum computers. These near term quantum computers are called noisy intermediate scale quantum (NISQ) devices.² The current largest quantum computer has just over 6,000 physical qubits.³ While the large number of qubits represents a substantial increase over the quantum computers from just a few years ago that had less than 100 qubits, it is still far from the number of qubits required to demonstrate quantum advantage. To solve a fully quantum algorithm for classically intractable systems, such as homogeneous

catalysis with a (60,60) active space, requires millions of physical qubits.⁴ An example of a fully quantum algorithm for deployment solely on quantum hardware is the Quantum Phase Estimation (QPE) algorithm designed to estimate the eigenvalues of a unitary operator, focused on solving for the electronic Schrödinger equation in quantum chemistry applications.^{5,6} QPE leverages the quantum Fourier transform (QFT) and phase kickback to extract the phase, or eigenvalue, of a unitary operator (\hat{U}), derived from the Hamiltonian (\hat{H}) via time evolution, $\hat{U} = e^{-i\hat{H}t}$. QPE computes the phase (θ_j) of the trial state $,|\psi\rangle$, which produces the energy eigenvalue, E_j , through the equation $\theta_j = -E_j t$. The QPE procedure begins by preparing the trial state $,|\psi\rangle$, often a Hartree-Fock or VQE reference, on a quantum computer. The auxiliary qubits are initialized in a superposition followed by controlled applications of the unitary operator $\hat{U} = e^{-iHt/\hbar}$. An inverse QFT is then applied to the qubits, and measurement of the system produces the binary representation of the phase θ_j . By applying \hat{U} to Schrödinger's equation, the energy can be found by:

$$E_j = 2\pi\hbar\theta_j \quad (1)$$

This approach offers exponential speedup over classical methods for computing the eigen-spectrum of unitary operators, particularly for strongly correlated systems.⁷ QPE is theoretically capable of demonstrating quantum advantage for large molecular systems when fault-tolerant quantum computers become available.⁴ However, QPE's practical implementation on current Noisy Intermediate-Scale Quantum (NISQ) devices is severely limited by its resource requirements. The algorithm requires deep quantum circuits requiring up to millions of qubits for error correction due to qubit decoherence.^{8,9} These requirements far exceed the capabilities of existing quantum computers. Despite these challenges, QPE remains a large focus for quantum chemistry applications due to its potential for exponential speedup and high accuracy. Recent efforts have focused on reducing its resource demands, such as iterative QPE variants that decrease the number of auxil-

iary qubits¹⁰ or hybrid approaches combining QPE with variational quantum eigensolver (VQE).¹¹ These advancements aim to bridge the gap between QPE's theoretical goals and practical implementation, particularly for future fault-tolerant quantum computers.

One solution to the limitations of NISQ devices is to derive hybrid algorithms that utilize both quantum and classical hardware. Two examples of these hybrid quantum computing algorithms are Quantum Select Configuration Interaction (QSCI) and the Variational Quantum Eigensolver (VQE).^{12,13} QSCI is a hybrid quantum algorithm inspired by the classical configuration interaction (CI) method. QSCI aims to approximate the ground and excited states of a molecular Hamiltonian by constructing a wave function as a linear combination of selected Slater determinants (electronic configurations), chosen based on the strength of contribution to a system's correlation energy. Unlike the full configuration interaction (FCI), which scales exponentially with system size, QSCI selectively includes only the most significant configurations, reducing computational complexity while retaining the electronic information most important to the chemical system. The classical CI wave function is expressed as:

$$|\psi\rangle = \sum_i c_i |\phi_i\rangle \quad (2)$$

where $|\phi_i\rangle$ are Slater determinants and c_i are variational coefficients optimized to minimize the energy, $\langle\psi|\hat{H}|\psi\rangle$. For QSCI the Hamiltonian is mapped to a qubit representation using transformations like Jordan-Wigner mapping,¹⁴ and the wave function is prepared as a superposition of computational basis states (Slater determinants). The subset of electronic configurations are selected by iteratively sampling the superposition of basis states to generate sets of the most frequently measured basis states.¹² The basis states with frequency above a user defined cutoff value are included in the reduced Hamiltonian (\mathbf{H}_R). The energy from the selected CI determinants (E_R) can then be calculated on the classical computer by application of the reduced Hamiltonian to the expansion coefficients \mathbf{c} by:

$$\mathbf{H}_R \mathbf{c} = E_R \mathbf{c} \quad (3)$$

One of QSCI's advantages is that the method is considered noise resilient and does not necessitate noise correction algorithms that other methods such as QPE and VQE require sometimes require. Noise on the quantum computer can indirectly affect the quality of the calculation through choosing unimportant configurations or neglecting some configurations that are important to accurately describe the system. The key to the noise resilience comes from the formation of the molecular Hamiltonian not being formed on the quantum computer where it can be subject to noise, but on the classical computer. This means that QSCI does not utilize quantum computers to solve for the wave function or energy of a system, but only to select the states that give the largest contributions to the correlation energy. Therefore, the QSCI eigenstates and eigenvalues are exact for the reduced Hamiltonian produced through the selected electronic configurations on the quantum computer by avoiding further use of NISQ devices and relying on classical hardware. The result of the exactness of the diagonalized Hamiltonian is that QSCI rigorously follows the variational principle. Compared to VQE, QSCI requires fewer variational parameters for a given accuracy but demands a much more complex state preparation to encode the multi-determinant wave function. The complex state preparation often requires using methods such as VQE to generate sufficiently accurate starting wave functions which increases the computational cost for increasingly large system sizes.¹² Furthermore, it has been shown that QSCI does not always produce accurate results more efficiently than the fully classical selective CI (SCI). The inefficiency of QSCI is in part driven by the nature of the state sampling which has been shown to produce a less compact wave function with more selected determinants for the same computed energy compared to classical SCI resulting in higher computational cost required to diagonalize the Hamiltonian matrix. QSCI can often require even more iterations to generate an accurate set of determinants because the search for new states can converge to already found states requiring further

state searches.¹⁵ Recent advancements, such as adaptive configuration selection,¹⁶ aim to improve QSCI's efficiency and robustness, making it a promising approach for quantum chemistry simulations on near-term and future quantum hardware.

The Variational Quantum Eigensolver (VQE) is a hybrid quantum-classical algorithm designed to approximate the eigenvalues of a Hamiltonian, with particular relevance to quantum chemistry and materials science.¹³ Unlike fully quantum algorithms, such as QPE, which demand fault-tolerant quantum hardware with millions of high-fidelity qubits, VQE is tailored for Noisy Intermediate-Scale Quantum (NISQ) devices.² NISQ devices, characterized by limited qubit counts and significant noise, are the current phase of quantum computing hardware. VQE constructs a parameterized trial wave function, or ansatz, which is prepared on a quantum computer. The expectation value of the Hamiltonian is then computed, and a classical optimizer iteratively adjusts the parameters to minimize the energy following the variational principle. This process is illustrated in Figure 1. This hybrid approach reduces the quantum circuit depth compared to fully quantum algorithms, trading off fewer quantum resources for increased classical optimization and measurement demands.¹⁷ Unlike QSCI, VQE relies on quantum hardware to generate the wave function and calculate the energy. The Hamiltonian is mapped onto a qubit representation using transformations like Jordan-Wigner mapping.¹⁴ The energy is evaluated as:

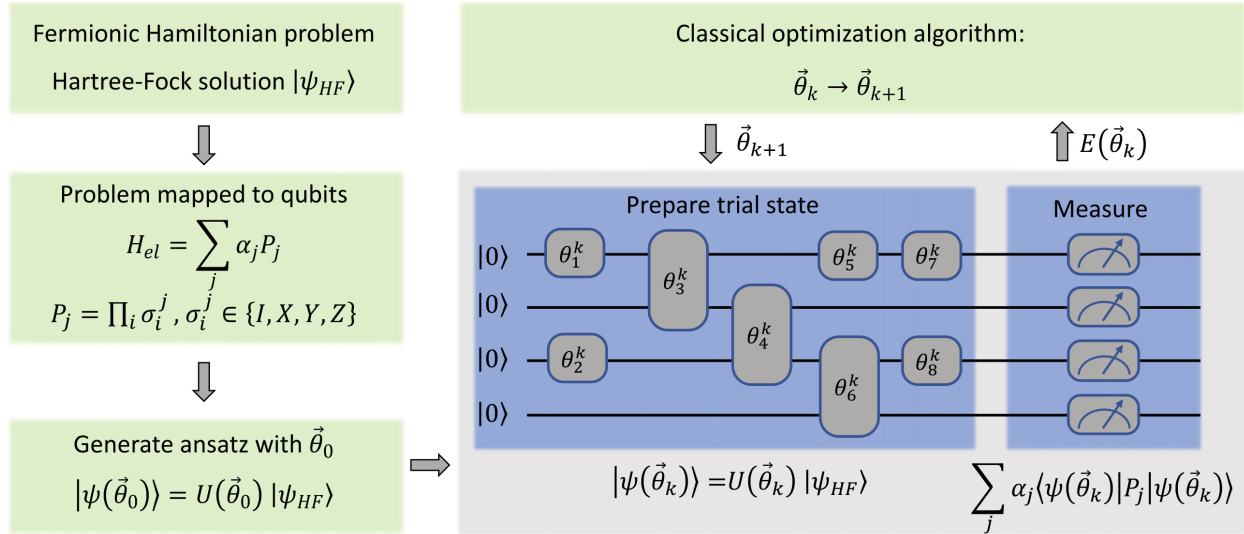
$$E(\vec{\theta}) = \langle \psi(\vec{\theta}) | \hat{H} | \psi(\vec{\theta}) \rangle \quad (4)$$

where \hat{H} is the qubit Hamiltonian, $|\psi(\vec{\theta})\rangle$ is the trial wave function parameterized by $\vec{\theta}$, and $E(\vec{\theta})$ is eigenvalue (energy) of the system. While \hat{H} can be written in first quantization representation, the methods considered in this overview are built upon the second quantization representation of the Hamiltonian:

$$\hat{H} = \sum_{p,q} h_{pq} a_p^\dagger a_q + \sum_{p,q,r,s} h_{pqrs} a_p^\dagger a_q^\dagger a_r a_s \quad (5)$$

where a_p^\dagger and a_p are the operators that act upon the orbital p to excite or de-excite the electrons from the molecular orbitals. These are called the creation and annihilation operators respectively. The one and two electron integrals, h_{pq} and h_{pqrs} respectively, are easily calculated on classical computers as a part of the state preparation usually through solving the Hartree-Fock equations.

Figure 1: General schematic of the VQE algorithm, showing the fermionic to qubit Hamiltonian mapping and highlighting the interplay between classical and quantum computers. The first step is to map the fermionic Hamiltonian calculated through a Hartree-Fock calculation to a qubit representation of the Hamiltonian. The ansatz is initialized with starting parameters $\vec{\theta}_0$. The ansatz is then prepared on the quantum computer as a set of gates. This begins the iterative cycle between the quantum and classical computers. Adapted from reference¹⁸ Copyright 2022 by Springer Nature under the Creative Commons CC BY license.



Several other mappings besides the aforementioned Jordan-Wigner mapping can be used to map \hat{H} to the qubits of a quantum computer. The two other most popular mapping methods are Bravyi-Kitaev and parity.^{19,20} This will map the second quantization fermionic operators of the Hamiltonian to qubit operators that can be deployed on quan-

tum hardware. The resultant qubit Hamiltonian can be represented as:

$$\hat{H} = \sum_j \alpha_j P_j = \sum_j \alpha_j \prod_i \sigma_i^j \quad (6)$$

Where α_j are scalar coefficients that have been mapped from h_{pq} and h_{pqrs} and P_j are Pauli strings that are formed by the product of Pauli matrices, σ_i^j . The Pauli matrices are the qubit creation and annihilation operators that have been mapped from the respective second quantization operators. Combining the qubit Hamiltonian with the energy expectation value, the quantum computer measures the energy of the system by:

$$E(\vec{\theta}) = \sum_j^N \alpha_j \langle \psi(\vec{\theta}) | \prod_i \sigma_i^j | \psi(\vec{\theta}) \rangle \quad (7)$$

This energy expression is analogous to the classical formulation of second quantization representation where the one and two electron integrals can be treated as scalar quantities:

$$E = \sum h_{pq} \langle \psi | a_p^\dagger a_q | \psi_0 \rangle + \sum h_{pqrs} \langle \psi | a_p^\dagger a_q^\dagger a_r a_s | \psi_0 \rangle \quad (8)$$

VQE's flexibility stems from the choice of ansatz, which influences both the quantum circuit complexity and the classical optimizations. The variety of different ansatz options are determined by how the different methodologies form the sets of excitation operators built from the creation and annihilation operators. Several ansatz generation schemes are studied in this work. The two primary ansatz categories used in VQE research are: chemistry-inspired ansatzes, such as the Unitary Coupled Cluster (UCC) method which aim to retain the electronic structure of the system, and hardware-efficient ansatzes, designed to minimize circuit depth by leveraging hardware level efficiencies of NISQ devices at the cost of losing physical symmetries.

For chemistry applications the chemistry-inspired ansatz is often the best choice for VQE since it retains the electronic structure and physical symmetries of a chemical prob-

lem. The UCC ansatz is the most chemically intuitive ansatz given its relationship to the standard coupled cluster equations, and is the basis for the original VQE method by Peruzzo et.al.¹³ The trial ansatz used for standard VQE calculations is the unitary coupled cluster with singles and doubles (UCCSD) ansatz which is the unitary version of the standard, classical CCSD method. A unitary ansatz is required since the total probability of the quantum state must be preserved. The UCCSD ansatz begins with solving the Hartree-Fock wave function. As with standard CCSD operator ($e^{\hat{T}}$), the unitary cluster operator ($e^{\hat{T}-\hat{T}^\dagger}$), is then applied to the ground state wave function:

$$|\psi(\vec{\theta})\rangle = e^{\hat{T}-\hat{T}^\dagger} |\phi\rangle \quad (9)$$

where the cluster operator, \hat{T} , is the sum of excitation operators with excitation levels indexed by i

$$\hat{T} = \sum_i T_i \quad (10)$$

Truncation of the cluster operator determines the excitation level of coupled cluster theory. UCCSD requires truncation of $T=2$ leading to

$$\hat{T}_{UCCSD} = \sum_i t_i^a a_p^\dagger a_q + \sum_{ij} t_{ij}^{ab} a_i^\dagger a_j^\dagger a_a a_b \quad (11)$$

Here the indices i,j,k,\dots and a,b,c,\dots denote occupied and virtual molecular orbitals respectively and t_i^a and t_{ij}^{ab} are the cluster amplitudes. This standard formulation of the UCCSD excitation scheme can be unfavorable in the number of qubits and gates required for a solution on the quantum computer. Many methods have been derived to reduce the number of excitation operators by recognizing that many of these excitations produce near zero contributions to the correlation energy, and therefore, can be neglected with little impact to the overall accuracy of the method. Some of these complexity reduction schemes are the focus of this work.

VQE’s hybrid nature makes it a practical stepping stone toward attaining quantum advantage in chemistry. Unlike QSCI, the accuracy of VQE is not as dependent on the quality of state preparation and has been consistently shown to provide accurate results more efficiently than the classical counterparts.

This paper is organized as follows. In section 2, we discuss several complexity reduction algorithms applied to VQE. These include circuit complexity reduction, chemistry optimized VQE methods, and extension of VQE to excited state methods. Section 3 presents a benchmarking of different circuit complexity reduction VQE methods. Section 4 lays out a brief overview of quantum computer simulators and related software packages. Lastly, in Section 5 the conclusions of our work are presented.

2 Circuit Complexity Reduction Methods

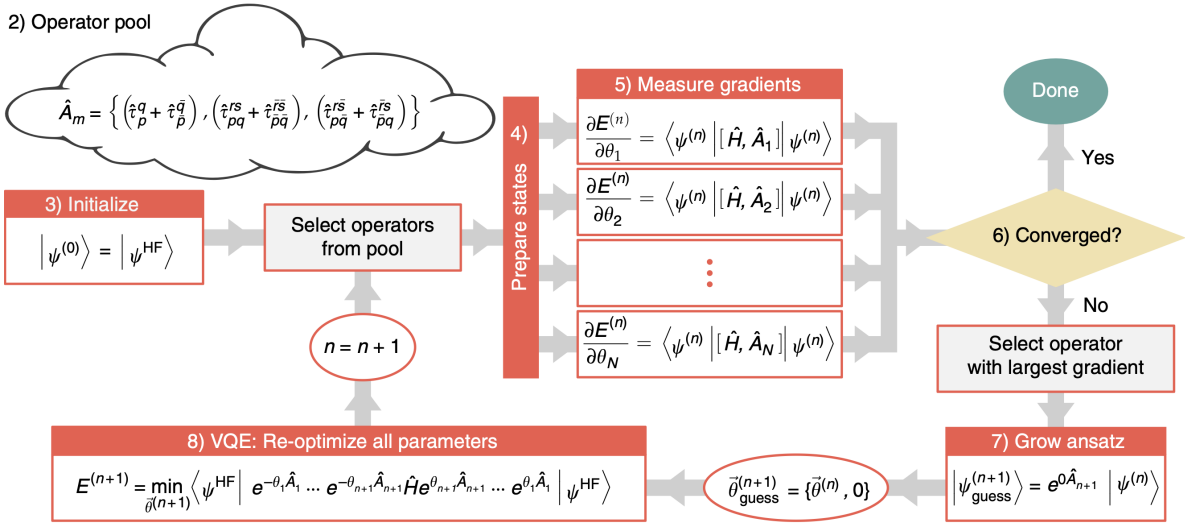
The following methods are examples of circuit complexity reduction methods. Circuit complexity methods are focused on ways to reduce the number of qubits, operators, gate depth, transistors, etc. on the quantum computer. In the NISQ stage of quantum computers, minimizing the number of gates and gate depth leads to a decrease in the effect of noise and decoherence on the results of the calculations. The decrease in quantum computing resources can often come at the cost of an increase in classical computing resources or an increase in the number of iterations.

2.1 ADAPT-VQE

The Adaptive Derivative-Assembled Pseudo-Trotter Variational Quantum Eigensolver (ADAPT-VQE) is a variation of the VQE method designed to recover most of the correlation energy utilizing the least number of fermionic operators and variational parameters.²¹ Unlike many VQE approaches that are built upon ansatzes with a fixed number of operators, ADAPT-VQE dynamically builds the ansatz by iteratively selecting operators

from a predefined pool based on the contribution to the energy gradient. This dynamic approach aims to minimize circuit depth and gate count, making it particularly suitable for NISQ hardware with limited coherence times.²

Figure 2: The ADAPT-VQE algorithm begins on the quantum computer by generating a pool of the possible qubit operators. The computed VQE ansatz is grown by one operator per iteration. The operator with the largest contribution to the correlation energy (determined by magnitude of the measured gradient) is added each iteration. This pattern is continued, and the ansatz grown, until the convergence tolerance is satisfied. This algorithm neglects terms with near zero contributions to the energy, reducing ansatz size without sacrificing accuracy. Adapted from reference.²¹ Copyright 2019 by Nature Communication under the Creative Commons CC BY license.



At the start of each iteration ADAPT-VQE evaluates the gradient of the energy with respect to each operator from the predefined pool of all potential operators:

$$\frac{\partial E}{\partial \theta_k} = \langle \psi | [\hat{H}, \hat{t}_k] | \psi \rangle, \quad (12)$$

where \hat{H} is the molecular Hamiltonian, \hat{t}_k is the sum of fermionic operators, and θ_k are the variational parameters. The operator with the largest gradient magnitude for a given iteration is added to the ansatz and a full VQE optimization of all current parameters is done. This process of iteratively adding operators to the ansatz repeats until the con-

vergence criteria are met when the norm of the gradient, $\|\vec{g}\|$, drops below a predefined threshold as shown in Figure 2.²¹

$$\|\vec{g}\| = \sqrt{\sum_i \left(\frac{\partial E}{\partial \theta_i}\right)^2} \quad (13)$$

One main advantage of ADAPT-VQE lies in its ability to reduce the size of the ansatz for specific molecular system through reducing the number of variational parameters and quantum gates. Unlike standard VQE, the underlying ansatz used for ADAPT-VQE is the generalized UCCSD ansatz which does not require excitations to be from occupied to virtual, but spans a general excitation space. This allows for a larger number of possible excitations and can capture some important excitations missing from the standard UCCSD used for many flavors of VQE. Simulations on small molecules like LiH and BeH₂ have shown that ADAPT-VQE can achieve chemical accuracy (within 1 kcal/mol of a full CI (FCI) calculation) with significantly fewer operators than UCCSD, often by an order of magnitude. Standard UCCSD-VQE failed to achieve chemical accuracy on the PES of BeH₂ apart from around equilibrium geometry while ADAPT-VQE was able to remain below chemical accuracy across the full PES. Futhermore, ADAPT-VQE attained this accuracy while using a fraction of the parameters (30 parameters) compared to UCCSD-VQE(120 parameters).²¹ Recent developments have focused on improving ADAPT-VQE's efficiency, such as using qubit-ADAPT-VQE, which employs a pool of Pauli operators to reduce circuit complexity.²² ADAPT-VQE has inspired other iterative quantum computing algorithms such as unitary selective coupled cluster (USCC) (Federov 2018) and the complete active space inspired CAS-VQE-SCF.²³

2.2 qADAPT-VQE

The qubit-Adaptive Derivative-Assembled Pseudo-Trotter Variational Quantum Eigensolver (qubit-ADAPT-VQE) builds on the ADAPT-VQE framework aiming to further re-

duce the quantum circuit complexity.²² In contrast to ADAPT-VQE which constructs the ansatz by selecting fermionic operators from a predefined pool, qubit-ADAPT-VQE selects operators from a pool of Pauli string operators. These Pauli strings are constructed from the strings generated within the fermionic pool. Compared to standard ADAPT-VQE, qubit-ADAPT-VQE reduces the number of multi-qubit gates, such as controlled NOT (CNOT) gates, which are prone to high error rates on NISQ computers.² By constructing the ansatz directly in the qubit space, qubit-ADAPT-VQE avoids the overhead of mapping fermionic operators, which often require long strings of these multi-qubit gates, but at the cost of a much larger number of variational parameters. In essence, by generating a pool of operators from qubit space, some of the computational load is being migrated from the quantum computer to the classical computer. As with fermionic ADAPT-VQE, the operators are added from an operator pool through the computation of the gradient of the energy with respect to the variational parameters. Benchmarks demonstrate that qubit-ADAPT-VQE achieves chemical accuracy with fewer gates than ADAPT-VQE or UCCSD, often reducing the CNOT counts by up to 50 percent for the same level of accuracy.²² Recent developments in qubit-ADAPT-VQE include further method to optimize the operator pool, such as pre-screening Pauli strings based on physical symmetries.²⁴ These improvements have been shown to work well for molecules like BeH₂, where qubit-ADAPT-VQE achieves near-full configuration interaction accuracy with significantly reduced quantum resources.²²

2.3 nu-VQE

The Non-Unitary Variational Quantum Eigensolver (nu-VQE) is another flavor of VQE, designed to improve the accuracy of electronic structure calculations on NISQ devices without increasing quantum circuit depth.²⁵ Unlike traditional VQE methods, which rely on unitary transformations to construct trial wave functions, nu-VQE introduces a non-unitary operator to increase quality of state representation without deepening quantum

circuits. The non-unitary operator applied in to the nu-VQE ansatz is the Jastrow operator inspired by the classical Quantum Monte Carlo (QMC) technique. This results in a hybrid quantum-classical method that improves energy estimates and provides an error mitigation effect on noisy devices.

In nu-VQE, the trial wave function is expressed as a non-normalized ansatz resulting from the application of a non-unitary operator $\hat{O}(\vec{\lambda})$ followed by a unitary operator $\hat{U}(\vec{\theta})$ on an initial state $|\Psi_0\rangle$:

$$|\Psi_O(\vec{\theta})\rangle = \hat{O}(\vec{\lambda})\hat{U}(\vec{\theta})|\Psi_0\rangle \quad (14)$$

where $|\Psi_0\rangle$ is typically the Hartree-Fock state, and $\vec{\theta}$ and $\vec{\lambda}$ are variational parameters for the unitary and non-unitary operators, respectively. The energy is computed by:

$$E = \frac{\langle \Psi_O(\vec{\theta}) | \hat{H} | \Psi_O(\vec{\theta}) \rangle}{\langle \Psi_O(\vec{\theta}) | \Psi_O(\vec{\theta}) \rangle} \quad (15)$$

which can be explicitly expressed as:

$$E = \frac{\langle \Psi(\vec{\theta}) | \hat{O}^\dagger(\vec{\lambda}) \hat{H} \hat{O}(\vec{\lambda}) | \Psi(\vec{\theta}) \rangle}{\langle \Psi(\vec{\theta}) | \hat{O}^\dagger(\vec{\lambda}) \hat{O}(\vec{\lambda}) | \Psi(\vec{\theta}) \rangle} \quad (16)$$

where $|\Psi(\vec{\theta})\rangle = \hat{U}(\vec{\theta})|\Psi_0\rangle$. The parameter $\vec{\theta}$ and $\vec{\lambda}$ are optimized in a standard fashion on classical computers.²⁵

The non-unitary operator used in nu-VQE is the Jastrow operator from classical QMC techniques for strongly correlated electrons. The Jastrow operator is generated at the qubit level after fermion to qubit mapping. The linearized approximate form for the inclusion of the one-body and two-body factors are given as:

$$\hat{J}(\vec{\alpha}, \vec{\lambda}) = 1 - \sum_{i=1}^N \alpha_i Z_i - \sum_{i < j=1}^N \lambda_{i,j} Z_i Z_j \quad (17)$$

where Z_i are single-qubit Pauli-Z operators, and α_i and $\lambda_{i,j}$ are variational parameters.

Utilizing the non-unitary Jastrow factor reduces circuit depth while increasing the accuracy of the VQE method, achieving chemical accuracy with shallower circuits compared to traditional VQE.²⁵

nu-VQE offers several advantages over standard VQE methods. Calculations on standard test systems, such as H₂, demonstrate that nu-VQE produces ground state energies with an absolute error an order of magnitude smaller than traditional VQE. nu-VQE faces some challenges on NISQ devices. The larger number of measurements required to optimize the Jastrow operators introduces a higher shot count compared to standard VQE methods which can generate higher statistical errors as system sizes grow.²⁶

Recent efforts have focused on utilizing nu-VQE as base method for localized active space methods that aim to capture non-dynamical correlation, namely the local active space nu-VQE (LAS-nu-VQE). LAS-nu-VQE utilizes the non-unitary operators to capture the interfragment correlations created by the fragmentations of the localized active spaces. This method has been used to study systems such as square cyclobutadiene.²⁷

2.4 USCC

Similar to ADAPT-VQE, unitary selective coupled cluster (USCC) is an alternative strategy to create a more compact ansatz that accurately describes the system while bypassing operators with near zero contributions to the correlation energy. Unlike ADAPT-VQE which has a screening criterion based on performing energy gradient calculations on each variational parameter, USCC sorts the operator pool through a prescreening criteria on the classical computer. This prescreening procedure is inspired by selected heat-bath configuration interaction²⁸ adapted to VQE operators. The energy gradient screening procedure of ADAPT-VQE requires $O(N^4)$ measurements per iteration on the quantum processor, while USCC avoids such overhead through a classical screening which is zero-cost on quantum hardware.¹⁸

The USCC prescreening method begins by generating all single and double excitations

from the reference, generally a Hartree-Fock wave function. Each single and double excitations are selected elements of the Hamiltonian matrix elements $h_1[i, a]$ or $h_2[i, j, a, b]$ that exceed a threshold ϵ_1 . The elements of the Hamiltonian matrix are operators consisting of contracted CC amplitudes and 1- and 2-electron integrals. Higher-order disconnected excitations (triple and quadruple) are added iteratively by correct contractions of the $h_1[i, a]$ or $h_2[i, j, a, b]$ and the t_1 or t_2 amplitudes. For example, an element of $h_2[i, j, a, b]$ can be formed by $t[i, j, a, b]h_1[k, c]$. Contracting this element of h_2 with $t[k, l, c, d]$ generates a disconnected quadruple excitation. These higher order excitations are added to the ansatz only if the values are larger than the defined thresholds. Thresholds are reduced (e.g., $\epsilon_n = \frac{\epsilon_{n-1}}{2}$) for each iteration, ensuring systematic inclusion of important terms.¹⁸

USCC's primary advantage is its ability to construct compact ansatzes without extra quantum resources, as the prescreening is classical. For systems in which standard UCCSD-VQE results in below chemical accuracy with the STO-3G basis USCCS is shown to achieve the same chemical accuracy with fewer parameters than UCCSD. For example, USCC requires 3X less parameters for H₂O than standard UCCSD-VQE. For systems (such as symmetric H_6) where UCCSD-VQE is above the chemical accuracy threshold, USCC is able to recover the missing correlation energy to achieve chemical accuracy through the included disconnected triple and quadruple excitations though these inclusions come at the high cost of increasing gate counts. Energy errors decrease systematically with ansatz size driven by lower threshold values which include more operators into the ansatz. Symmetry-based prescreening further reduces operators by up to a factor of 3 without accuracy loss.

2.5 Other VQE flavors

In the fast pace field of VQE ansatz development for NISQ devices, there is an overabundance of novel methods being published that focus on circuit complexity reduction. The VQE flavors highlighted in this overview represent those that were most interesting to

us. While not an exhaustive list, other available VQE flavors are presented here without in-depth analysis. Dual-VQE is a method that creates a lower bound to the ground state energy of a system designed to be a check against the upper bound limit of standard VQE.²⁹ Overlap-ADAPT-VQE modifies the operator selection algorithm to avoid the traps of local minima that can lead to over parameterized wave functions.³⁰ Greedy gradient free adaptive VQE (GGA-VQE) is a gradient free adaptive ansatz growth algorithm that aims to create noise resilience by avoiding gradient calculations.³¹ Amplitude Reordering ADAPT-VQE (AR-ADAPT-VQE) utilizes amplitude reordering to batch accumulate operators into the ansatz to accelerate convergence.³² Zhang et. al. added a denoising diffusion model to the VQE algorithm to address issues with iteration demands and local minima issues.³³ Wang et. al. work to improve standard VQE by replacing the vanilla gradient (VG) with the quantum natural gradient descent (QNG) for faster convergence.³⁴ VQE-CVQE is a hybrid algorithm that combines standard VQE with cascaded VQE (CVQE) using diabatic state preparation to generate long term error correction.³⁵

3 Chemistry Inspired Methods

This section focused on chemistry inspired methods that utilize VQE as a portion of a larger scheme to recover more electronic information including non-dynamical correlation. These methods also include fragmentation methods combined with VQE to decrease the problem size deployed onto quantum computers. Fragmentation methods have been used classically to reduce computational cost and complexity, but at the cost of losing some inter-fragment correlation.

3.1 ClusterVQE

The ClusterVQE algorithm is another method designed to reduce the circuit depth and the number of qubits required for VQE.³⁶ Unlike standard VQE approaches, which oper-

ate on the full qubit space, ClusterVQE partitions the qubits into clusters which are distributed across shallower, independent quantum circuits. These clusters are partitioned based on mutual information that maximizes correlation within clusters and minimized correlations between clusters. The inter-cluster effects are handled by a dressed Hamiltonian, enabling exact simulation with fewer quantum resources at the expense of additional classical computation.

In ClusterVQE, the qubit space is divided into clusters where each cluster is assigned to a separate quantum circuit. The clusters are determined by maximizing intra-cluster mutual information (MI) in a fashion similar to that of the classical density matrix renormalization group (DMRG) method.³⁷ The initial reduced density matrix for the system is obtained from the classical Hartree-Fock calculation. From here the clustering uses a classical graph partitioning algorithm to minimize the sum of inter-cluster mutual information. Inter-cluster correlations are incorporated by dressing the Hamiltonian, H_d , with an entangler $\hat{U}_{c_{ij}}$ that connects cluster i with cluster j .³⁶

$$\hat{H}_d = \Pi_{i \neq j} \hat{U}_{ij}^\dagger \hat{H} \hat{U}_{ij} \quad (18)$$

By dressing the Hamiltonian with the inter-cluster entanglers, the clusters can be mapped to sets of smaller qubits that represent each cluster resulting in much shallower qubit depth. This comes at the cost of increased classical resources required to update the dressed Hamiltonian.

ClusterVQE's key advantage is its ability to simulate larger systems with reduced quantum hardware demands. For LiH (8 qubits, STO-3G basis), it achieves chemical accuracy with clusters of 4 qubits each, using circuits 2–3 times shallower than qubit-ADAPT-VQE and requiring fewer iterations than iQCC.³⁸ As with ADAPT-VQE (both fermionic and qubit), ClusterVQE iteratively grows the ansatz by comparing contributions of each operator to the correlation energy using analytic gradients. ClusterVQE can be limited by the classical optimization of clustering and the iterative dressing which in-

introduce additional computational overhead, scaling with system size and cluster count. For strongly correlated systems, incomplete capture of inter-cluster entanglement may lead to convergence issues, requiring more iterations.

3.2 FMO

The Fragment Molecular Orbital-Based Variational Quantum Eigensolver (FMO-VQE) is a hybrid quantum-classical algorithm that integrates the fragment molecular orbital (FMO) method with the Variational Quantum Eigensolver (VQE) to enable scalable quantum chemistry simulations.³⁹ Traditional VQE faces limitations in qubit count and noise for large molecules. FMO has been used with fully-classical quantum chemistry methods for many years to increase the scalability of these methods to large systems.⁴⁰ FMO divides systems into independent fragments, decreasing the computational cost of large systems to a larger number of smaller problems.

In FMO-VQE, the molecular system is fragmented into sets of monomer and dimers (often up to trimers in the fully classical realm) where the total energy is approximated as:

$$E_{\text{FMO}} = \sum_I E_I + \sum_{I < J} \Delta E_{IJ} \quad (19)$$

where E_I is the energy of fragment monomer I computed via VQE in the presence of the electrostatic potential from the rest of the system, and ΔE_{IJ} is the dimer correlation energy.

$$\Delta E_{IJ} = E_{IJ} - E_I - E_J \quad (20)$$

where E_{IJ} is the energy of fragment dimer composed of monomers I and J computed via VQE in the presence of the electrostatic potential from the rest of the systems. Bond breaking across fragments is handled by either Hybrid Orbital Projection (HOP)⁴⁰ or Adapted Frozen Orbital (AFO).⁴¹

FMO-VQE's main advantage is its qubit efficiency, enabling simulations of large sys-

tems that require much smaller number of qubits. For H_{24} with the STO-3G basis (48 basis functions), FMO-VQE achieves an error of 0.053 mHa using 4 qubits for each monomer calculation and 8 qubits per dimer calculation. This is compared to the 48 qubits needed to run standard VQE on H_{24} . For H_2O with the 6-31G basis (80 basis functions) the resulting error is 1.376 mHa using 8 qubits for each monomer calculation and 16 qubits per dimer calculation. This is compared to the 80 qubits needed to run standard VQE on the same system.³⁹ The method retains chemical accuracy by including many-body effects via fragment interactions. However, FMO-VQE has limitations. Unless handled carefully, bond breaking required for fragmentation of many systems can result in errors for highly correlated systems.

3.3 ADAPT-VQE-SCF

The ADAPT-VQE Self-Consistent Field (ADAPT-VQE-SCF) method integrates the orbital optimization of the classical complete active space SCF (CASSCF) method within the ADAPT-VQE framework to enhance the efficiency of capturing non-dynamical correlation on NISQ devices.²³ Building on ADAPT-VQE, which iteratively grows an ansatz by selecting operators based on energy gradients, ADAPT-VQE-SCF incorporates a SCF loop to optimize molecular orbitals (MOs), minimizing energy errors with respect to orbital changes and capturing non-dynamical correlation.

The CASSCF method is a multi-configurational approach in quantum chemistry that simultaneously optimizes molecular orbitals and configuration interaction coefficients to capture the non-dynamical electron correlation in ground and excited states.^{42,43} Unlike single-reference methods like Hartree-Fock (the basis state for most VQE methods), CASSCF addresses systems with near-degenerate orbitals by defining an active space (CAS) of N electrons in L orbitals, denoted $CAS(N,L)$, where full configuration interaction (FCI) is performed.

In CASSCF, the wave function is expanded as:

$$|\Psi\rangle = \sum_I c_I |\phi_I\rangle \quad (21)$$

where $|\phi_I\rangle$ are Slater determinants from all distributions of N electrons in L orbitals, and c_I are CI coefficients. The energy is minimized variationally:

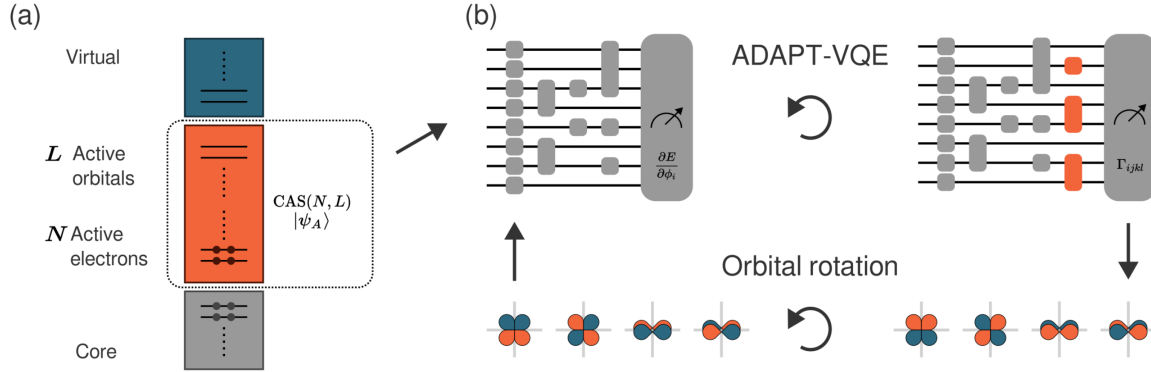
$$E = \min_{\mathbf{c}, \mathbf{C}} \langle \Psi | \hat{H} | \Psi \rangle \quad (22)$$

with \mathbf{c} the CI vector and \mathbf{C} MO coefficients, expanded as $\phi_p = \sum_\mu C_{\mu p} \chi_\mu$ in atomic orbitals χ_μ . Optimization alternates between CI diagonalization and orbital rotations.⁴²

ADAPT-VQE-SCF extends this by alternating between minimizing the CAS energy expectation value with VQE and the orbital optimization as illustrated in Figure 3. This allows the computationally demanding nature of the CI diagonalization to be offloaded to the quantum computer, while still allowing for the orbital relaxations. To fully optimize the convergence process, the ADAPT-VQE part of the calculation is not fully converged before orbital rotations. This process would converge to an accurate result, but it would become prohibitively expensive to run a full ADAPT-VQE algorithm every iteration. Instead, each iteration only adds 1 operator to the ansatz, followed by the VQE calculation, and then the orbital rotations. This decreases the overall computational work done by the quantum computer while still capturing the intended correlation energies.

ADAPT-VQE-SCF's key advantage is its ability to capture non-dynamical correlation. UCCSD, the ansatz for most all chemistry inspired quantum chemistry ansatz, captures dynamical correlation, but cannot account for the effects of multireference states. ADAPT-VQE-SCF captures this multireference character that is important for studying many transition metal containing catalytic complexes. For ferrocene $[\text{Fe}(\text{C}_5\text{H}_5)_2]$ with the cc-pVDZ basis (requiring 20 qubits), it achieves chemical accuracy with fewer parameters and shallower circuits when compared to UCCSD.²³ Orbital optimization captures

Figure 3: Schematic diagram of the ADAPT-VQE-SCF algorithm, highlighting the interplay between the solution of the wavefunction via VQE and the orbital optimization of CASSCF. Reproduced with permission from reference.²³ Copyright 2024 by American Chemical Society.



the non-dynamical correlation efficiently, outperforming non-optimized ADAPT-VQE by 5–10 mHa in transition-metal complexes. One limitation of ADAPT-VQE-SCF is its inability to capture dynamical correlation which are critical for predicting chemical reactions (e.g., reaction energies and barriers). In order to effectively capture both dynamical and non-dynamical correlation a multi-reference coupled cluster method aimed at quantum computers needs to be investigated.

3.4 LAS-nuVQE

The Localized Active Space Non-Unitary Variational Quantum Eigensolver (LAS-nuVQE) is a hybrid quantum-classical algorithm that combines the localized active space self-consistent field (LASSCF) method with a non-unitary variational quantum eigensolver (nuVQE) to simulate strongly correlated systems on NISQ devices.²⁷ Traditional VQE lacks multireference character for systems with near degenerate states. The Localized Active Space Self-Consistent Field (LASSCF) method is a multiconfigurational quantum chemistry approach that approximates CASSCF by localizing active spaces to molecular fragments, enabling efficient treatment of large systems with strong local correlation that

would be prohibitively expensive for full CASSCF.^{44,45}

In LASSCF, the system is partitioned into fragments, each with its own localized active space $\text{CAS}(N_I, L_I)$ for fragment I. The wave function is a product of fragment wave functions:

$$|\Psi_{\text{LAS}}\rangle = \bigwedge_I |\psi_I\rangle \quad (23)$$

where $|\psi_I\rangle = \sum_{J_I} c_{J_I} |\phi_{J_I}\rangle$ is the FCI expansion within fragment I's active space. Optimization self-consistently minimizes the energy:

$$E = \min_{\mathbf{c}_I, \mathbf{C}_I} \langle \Psi_{\text{LAS}} | \hat{H} | \Psi_{\text{LAS}} \rangle \quad (24)$$

with fragment-specific MO coefficients \mathbf{C}_I and interfragment mean-field embedding.

However, LASSCF scales with fragment size, limiting to moderate active spaces per fragment, and approximates long-range correlation via mean-field, potentially inaccurate for delocalized systems. One solution to the interfragment correlation is utilizing nuVQE (as previously discussed) as the single determinant method that spans the full active space of the system. LAS-nuVQE passes the converged LASSCF wave function into a hardware efficient ansatz on the quantum computer to recover interfragment correlation missed by the mean-field approach. LAS-nuVQE was shown to effectively recover this interfragment correlation with shallow circuits (70 gates), achieving chemical accuracy in H4 and cyclobutadiene (C4H4) using 4–8 qubits. It is also shown that LAS-nuVQE outperforms classical LASSCF when compared to FCI.²⁷ LAS-nuVQE faces challenges. Localization approximations may miss long-range correlations in delocalized systems. Compared to ADAPT-VQE-SCF, which optimizes orbitals adaptively but requires more measurements, LAS-nuVQE shifts complexity to classical LASSCF preprocessing. Unlike ADAPT-VQE-SCF, LAS-nuVQE does not iteratively alternate between capturing the interfragment correlation and orbital rotations. Just like fully classical CASSCF/LASSCF, while LAS-nuVQE does capture important non-dynamical correlation, it does not cap-

ture the dynamical correlation often needed to study reaction pathways and catalytic processes. Perturbative corrections such as second order perturbation theory (PT2) are needed to recover this dynamical correlation.

4 Excited state methods

Many chemically relevant problems, like spectroscopy, photochemistry, and excited-state reactivity, etc. require access to excited states. This section focuses on extensions of VQE for excited-state calculations that have been developed for excited-state calculations. These approaches aim to overcome challenges such as variational collapse, state orthogonality, and the accurate representation of electronically excited configurations within the variational framework.

4.1 Variational Quantum Deflation (VQD) method

The VQD algorithm, introduced by Higgott et al. is an extension of the VQE designed to compute excited-state energies of a Hamiltonian on near-term quantum devices.⁴⁶ It systematically finds the k -th excited state by adding overlap penalty terms to the VQE cost function, enforcing orthogonality between the target state and all previously obtained eigenstates.

In standard VQE, the ground-state energy is obtained by minimizing:

$$E(\theta) = \langle \psi(\theta) | \hat{H} | \psi(\theta) \rangle = \sum_j c_j \langle \psi(\theta) | P_j | \psi(\theta) \rangle \quad (25)$$

where $\hat{H} = \sum c_j P_j$ is the Hamiltonian expressed as a sum of Pauli operators.

In VQD, the cost function for the k -th excited state is modified as:

$$F(\theta_k) = \langle \psi(\theta_k) | \hat{H} | \psi(\theta_k) \rangle + \sum_{i=0}^{k-1} \beta_i |\langle \psi(\theta_k) | \psi(\theta_i) \rangle|^2 \quad (26)$$

where β_i is a manually chosen hyperparameter enforcing orthogonality to the ground state. The first part of the Eq. 26 is evaluated using standard VQE circuits, while the second term involves overlap measurements with previously obtained states. These overlaps, $|\langle\psi(\theta_i)|\psi(\theta_k)\rangle|^2$, can be efficiently estimated using low-depth circuits based on the relation $|\langle\psi(\theta_i)|\psi(\theta_k)\rangle|^2 = |\langle 0|R(\theta_i)^\dagger R(\theta_k)|0\rangle|^2$, where $R(\theta)$ prepares the ansatz state from $|0\rangle$. The overlap is determined from the fraction of all-zero measurement outcomes obtained from $O(1/\epsilon^2)$ samples. To mitigate device imperfections that affect the inverse circuit $R(\theta_i)^\dagger$, the inverse can be variationally reconstructed by optimizing parameters to maximize the overlap $|\langle 0|R(\theta_i)^\dagger R(\theta_i^*)|0\rangle|^2$. This approach preserves the robustness to control errors characteristic of VQE. VQD maintains the same qubit requirements as VQE and typically doubles the circuit depth due to overlap estimation. Low-depth overlap measurements can be performed using methods such as the destructive SWAP test or direct overlap estimation circuits. The algorithm is robust to control errors and compatible with common error mitigation techniques.

4.2 VQE with Spin-Restricted Ansatz and Automatically-adjusted constraints (VQE/AC)

An excited-state quantum algorithm that combines a spin-restricted ansatz with the VQE under automatically-adjusted constraints to improve accuracy and numerical stability on NISQ devices is developed by Gocho et al.⁴⁷ The VQE/AC method improves upon the variational quantum deflation (VQD) approach by eliminating the need to predefine constraint weights (β parameters) and instead employs the COBYLA optimization algorithm to automatically enforce orthogonality to lower states. This adaptive constraint handling enables smooth potential energy surfaces (PESs) without manual tuning of hyperparameters.

To enhance accuracy and mitigate spin contamination, the authors introduced a spin-restricted ansatz that constructs trial wave functions strictly within the subspace of a

given spin multiplicity (e.g., singlet), leading to shorter circuits and fewer variational parameters than heuristic ansatz. The approach was benchmarked for ethylene and phenol blue at their Franck–Condon (FC) and conical intersection (CI) geometries using CASSCF-level simulations. The method reproduced ground and excited-state energies with errors below 0.5 kcal mol⁻¹ on noisy simulators and within 2 kcal mol⁻¹ on IBM’s *ibm_kawasaki* device.

4.3 Folded Spectrum VQE

Folded spectrum (FS)-VQE is proposed as an extension of the standard VQE framework to compute the molecular excited states.⁴⁸ In the conventional VQE, the goal is to minimize the expectation value of the molecular Hamiltonian given by Eq. 25 where the parametrized trial wave function $|\psi(\theta)\rangle$ is prepared with a chosen ansatz on a quantum circuit. However, in FS-VQE, the minimization instead targets the expectation value of the FS operator $(\hat{H} - \omega)^2$ instead of the Hamiltonian \hat{H} , with ω being chosen as reference energy. By minimizing the FS operator, one derives an eigenstate of \hat{H} where the value of $(E_i - \omega)^2$ reaches its minimum. This results in an excited state of the Hamiltonian that closely aligns with the desired energy ω . The cost function is defined as

$$F = \langle \psi(\theta) | (\hat{H} - \omega)^2 | \psi(\theta) \rangle \quad (27)$$

and its minimization is carried out variationally within the VQE framework. The resulting wave function is an approximate eigenstate determined by the selected ansatz. By varying the parameter ω across the energy spectrum, different excited states can be systematically obtained. The ansatz employed is the Unitary Coupled Cluster (UCC) i.e.,

$$|\Psi_{UCC}\rangle = e^{\hat{T} - \hat{T}^\dagger} |\psi_o\rangle \quad (28)$$

with single and double excitation operators mapped to Pauli strings via the Jordan-Wigner transformation. The expectation values of the large number of Pauli terms arising in $(\hat{H} - \omega)^2$ are efficiently evaluated using Pauli reduction and grouping, which identifies sets of commuting Pauli strings that can be measured simultaneously. By employing Pauli grouping, it reduces the nominal $O(N^8)$ scaling of the squared Hamiltonian to an effective $O(N^6)$. It also incorporates error-mitigation techniques like zero-noise extrapolation (ZNE) and SPAM correction to improve robustness on noisy simulators.

4.4 Equation of motion based methods for excited states

Classical methods for excited state calculations often leverage linear response theory, most notably through Equation of Motion (EOM) formalisms (such as EOM-Coupled Cluster). EOM-based approaches are highly valued in quantum chemistry because they directly compute the energy difference between the excited state and an already optimized ground state, thereby naturally yielding size-intensive excitation energies. Furthermore, they provide a systematic way to include correlation effects and are robust across different regimes, making them a powerful theoretical framework to adapt for quantum computing.

The **Quantum Equation-of-Motion (qEOM)**, introduced by Ollitrault et al., adapts the classical EOM formalism to the constraints of a hybrid quantum-classical computing environment, offering an efficient extension of the VQE method for calculating molecular excitation energies.⁴⁹ The theoretical foundation for calculating the excitation energy, $E_{0n} = E_n - E_0$, is derived from the double commutator, which ensures the resulting energy differences are real and the operators are Hermitian. The core expectation value for the excitation energy is thus given by:

$$E_{0n} = \frac{\langle 0 | [\hat{O}_n, [\hat{H}, \hat{O}_n^\dagger]] | 0 \rangle}{\langle 0 | [\hat{O}_n, \hat{O}_n^\dagger] | 0 \rangle} \quad (29)$$

The excitation operator \hat{O}_n^\dagger is systematically expanded as a linear combination of basis excitation (\hat{E}) and deexcitation (\hat{E}^\dagger) operators, typically restricted to single and double electronic excitations for practical quantum implementation

$$\hat{O}_n^\dagger = \sum_{\mu} [X_{\mu\alpha}^{(\alpha)}(n) \hat{E}_{\mu\alpha}^{(\alpha)} - Y_{\mu\alpha}^{(\alpha)}(n) (\hat{E}_{\mu\alpha}^{(\alpha)})^\dagger] \quad (30)$$

Importantly, the inclusion of the deexcitation coefficients (Y) is what differentiates qEOM from methods based on the Tamm-Dancoff approximation, making it applicable to systems exhibiting strong correlation. Applying the variational principle to this formulation leads directly to the core mathematical challenge: a generalized secular equation that must be solved classically:

$$\begin{pmatrix} M & Q \\ Q^* & M^* \end{pmatrix} \begin{pmatrix} X_n \\ Y_n \end{pmatrix} = E_{0n} \begin{pmatrix} V & W \\ -W^* & -V^* \end{pmatrix} \begin{pmatrix} X_n \\ Y_n \end{pmatrix} \quad (31)$$

The implementation of qEOM is broken into sequential steps: first, a quantum processor runs the VQE routine to find the optimal ground-state parameters θ_0 ; second the quantum state $|\psi(\theta_0)\rangle$ is prepared again to efficiently measure the expectation values of the operators corresponding to the matrix elements (M,Q,V,W) and finally a classical computer constructs and solves the secular equation to obtain the excitation energies E_{0n} .

For systems where the Born-Oppenheimer approximation is invalid or insufficient, such as those involving photoinduced proton transfer or light particles like positrons, the **Multicomponent Equation-of-Motion (mcEOM)** method extends this framework.⁵⁰ The mcEOM, paired with the Multicomponent Unitary Coupled Cluster (mcUCC) ansatz, allows for the quantum mechanical treatment of multiple particle types (e.g., electrons and nuclei/positrons) simultaneously. This is achieved by formulating the excitation operator \hat{O}_n^\dagger to include both electronic and non-electronic particle excitations, leading to a secular equation identical in form to the standard EOM-CC method, but with much greater di-

mensionality due to the inclusion of all particle types. The resulting algorithm, mcEOM-VQE, is crucial for studying non-Born-Oppenheimer processes, where excitations can involve the simultaneous transition of electrons and quantum nuclei.

A further development is the **Quantum Self-Consistent Equation-of-Motion (q-sc-EOM)** method.⁵¹ This formalism, inspired by UCC-based excited-state methods, addresses key theoretical and practical limitations of both qEOM and the Quantum Subspace Expansion (QSE) by defining the state-transfer operator \hat{O}_k such that its action on the ground state generates the k -th excited state,

$$\hat{O}_k |\psi_{gr}\rangle = |\psi_k\rangle, \quad (32)$$

and by using self-consistent operators to enforce the vacuum annihilation condition (VAC) i.e., $\hat{O}_k |\psi_{gr}\rangle = 0$. By rigorously satisfying the VAC, q-sc-EOM provides highly accurate, strictly size-intensive, and guaranteed real energy differences, making it suitable for calculating not just Electronic Excitation Energies (EEs) but also Ionization Potentials (IPs) and Electron Affinities (EAs), which qEOM fails to do accurately. The advantages of using these self-consistent operators translate directly into major computational benefits. First, the self-consistency causes the overlap matrix V to become the identity matrix and the off-diagonal matrices Q and W to become zero, simplifying the problem to a standard, Hermitian eigenvalue problem:

$$MA_k = E_{0k} VA_k \quad (33)$$

This simplification removes the need to measure the complex, noise-sensitive overlap matrix V on the quantum computer. Second, this resource efficiency is amplified because the overall measurement protocol for the matrix M is simplified, strictly requiring only up to 2-body Reduced Density Matrices (RDMs). This is a significant improvement over QSE and qEOM, which require higher-body RDM measurements (up to 4-body or 12-qubit measurement strings), making q-sc-EOM theoretically expected to be far more resilient to hardware noise and more resource-efficient for implementation on NISQ devices.

To address the challenge of simulating systems with large basis sets on resource-limited hardware, the **Orbital-Optimized VQE - Quantum Equation-of-Motion (oo-VQE-qEOM)** protocol was introduced.⁵² This method is the quantum counterpart to the classical CASSCF-EOM approach. The foundational idea is to first optimize the ground state using oo-VQE, which minimizes the energy with respect to both the quantum circuit parameters ($\vec{\theta}$) and the classical molecular orbital rotation parameters ($\vec{\kappa}$). This is a coupled optimization problem over the total energy $E(\vec{\kappa}, \vec{\theta})$. The core strategy is the Active Space Approximation, which partitions the molecular orbitals into three sets: inactive (always occupied), virtual (always unoccupied), and active (correlated on the QPU). The active space approximation has the advantage that the qubits corresponding to inactive and virtual parts can be removed, and only the active space will be simulated on a quantum computer reducing the number of qubits and gates needed for the simulation. The Hamiltonian is then restricted to the active space, as shown:

$$\hat{H}(\vec{\kappa}) = \sum_{pq}^N h_{pq}(\vec{\kappa}) \hat{E}_{pq} + \frac{1}{2} \sum_{pqrs}^N g_{pqrs}(\vec{\kappa}) (\hat{E}_p q \hat{E}_{rs} - \delta_{qr} \hat{E}_{ps}) + h_{nuc} \quad (34)$$

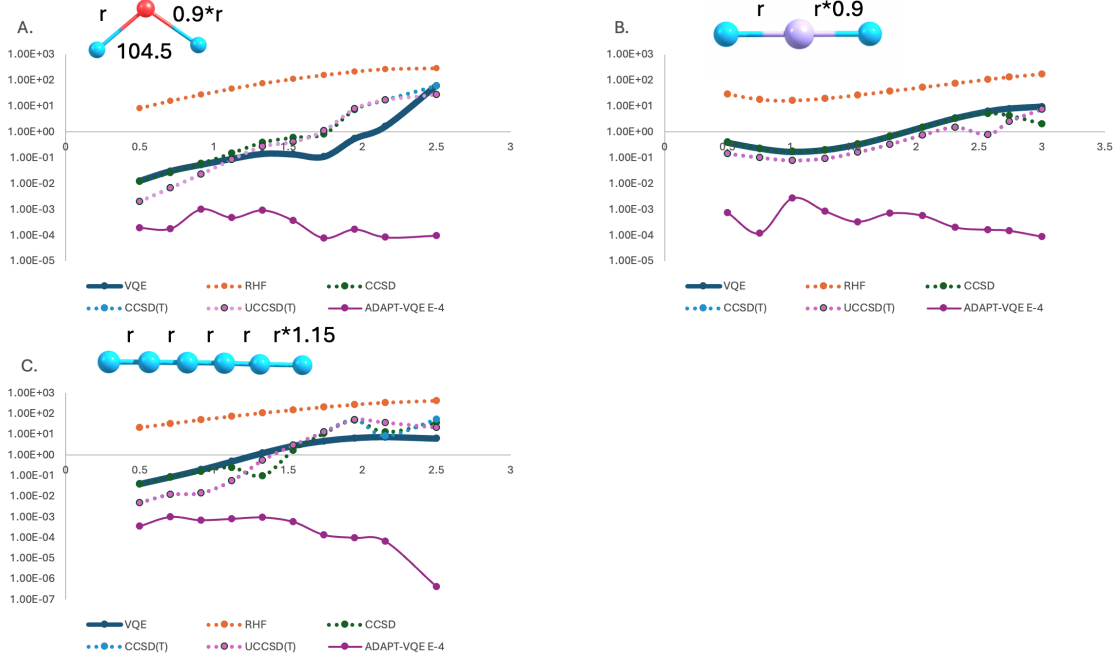
The orbital optimization step, controlled by $\vec{\kappa}$, effectively compacts the required correlation information into this smaller, measurable active space, thereby enabling larger basis sets to be treated while minimizing the qubit count. Following this optimization, the EOM secular equation is constructed using an extended set of excitation and de-excitation operators. active-space electronic excitations (\hat{G}_I) but allow orbital rotation operators (\hat{q}_I) that act between the active, inactive, and virtual orbital spaces. This integrated approach allows oo-VQE-qEOM to accurately compute not just excitation energies, but also complex properties like electronic absorption (oscillator strengths) and circular dichroism (rotational strengths), demonstrating good agreement with classical CASSCF and FCI benchmarks while remaining feasible for near-term quantum resources.

5 Benchmarking

The goal of the benchmarking efforts is to compare the accuracy of VQE to classical methods, comparing different flavors of VQE to one another, and to assess the basis set dependence on VQE methods. A range of classical methods applied to three molecules were used to assess the accuracy of UCCSD-VQE compared to classical methods. The computational details for the VQE flavors is given in the SI. Energies for restricted Hartree-Fock (RHF), coupled cluster with singles and doubles (CCSD) and non-iterative triples (CCSD(T)), and unrestricted CCSD(T) (UCCSD(T)) were calculated with the STO-3G basis set and errors against full configuration interaction (FCI) are reported in log scale for non-symmetric H_2O , non-symmetric BeH_2 , and non-symmetric H_6 in Figure 4. Errors for both standard UCCSD-VQE and ADAPT-VQE are plotted to compare the accuracy of these methods compared to classical methods including the so called "Gold Standard" classical method CCSD(T). Both restricted and unrestricted CCSD(T) are included to capture important information about potential unpaired electrons in the large bond stretching regions where energies errors often occur for methods built upon restricted HF methods. Only the largest values of R show any divergence between CCSD(T) and UCCSD(T). As expected the baseline method RHF has high errors well above chemical accuracy (1 kcal/mol) when compared to FCI. In the bonding regions around equilibrium all other methods have errors below chemical accuracy. Across the full potential energy surface (PES) for each molecule there is little differences between the errors in CCSD, CCSD(T), UCCSD(T), and standard VQE due to the underlying excitation schemes being the same between each one. ADAPT-VQE with a tight cutoff value shows much smaller errors across each PES compared to all other methods.

As shown in the preceding sections, many methods have been developed to decrease the number of qubits required by a VQE calculation by selecting the excitation operators that have the largest contributions to the correlation energy, ignoring the operators with

Figure 4: RHF, CCSD, CCSD(T), UCCSD(T), UCCSD-VQE and ADAPT-VQE (threshold ϵ^{-4}) energy differences from FCI plotted on a log scale for increasing interatomic distances with the STO-3G minimal basis set. The molecules tested are A. non-symmetric H_2O B. non-symmetric BeH_2 and C. non-symmetric H_6 .

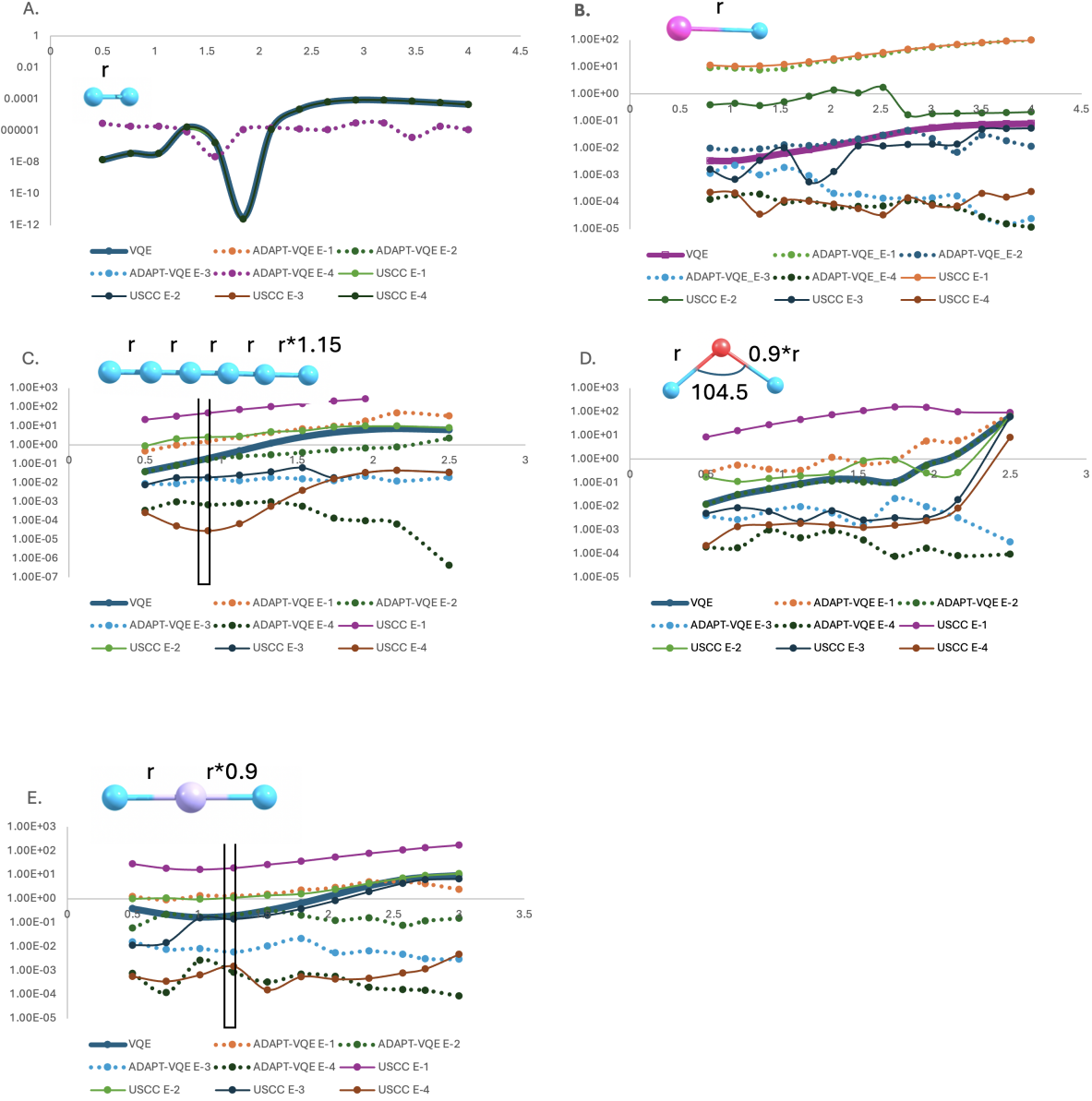


near zero contributions. Two distinct VQE based methods that rely on gradients to generate operator pools of highest contribution operators are ADAPT-VQE and USCC. Details of these algorithms are given in preceding sections. These two VQE flavors are compared to standard VQE with varying threshold values for both number of operators and accuracy compared to FCI as shown in Figure 5. Both ADAPT-VQE and USCC were run with thresholds of ϵ^{-1} , ϵ^{-2} , ϵ^{-3} , and ϵ^{-4} . For ADAPT-VQE with the STO-3G basis set a threshold value of ϵ^{-2} will achieve chemical accuracy across the PES for all but the largest bond stretches and a threshold value of ϵ^{-3} will produce errors below those of standard VQE across the PES. In the case of USCC the threshold ϵ^{-3} is required to be below chemical accuracy across the full PES for all but the largest bond stretches and for most of the molecules this threshold is enough to have smaller errors than standard VQE. The PES for BeH_2 requires a threshold cutoff of ϵ^{-4} for USCC to be more accurate than standard VQE

across the PES. The exception to the threshold values is the H_2 molecule where USCC for all thresholds are equivalent to standard VQE and all ADAPT-VQE thresholds generate the same errors. The small number of potential excitations for H_2 with the minimal basis set does not allow for a sufficient number of operators in the generated operator pool to distinguish between the various methods and threshold values. As a general recommendation for ADAPT-VQE with the STO-3G basis set, a threshold value of ϵ^{-2} will generate errors below chemical accuracy and ϵ^{-3} will produce more accurate results than standard VQE. Similarly, for USCC threshold values of ϵ^{-3} and ϵ^{-4} are required to produce accuracy below chemical accuracy and standard VQE respectively. At any point on the PES of the test molecules both ADAPT-VQE and USCC are capable of accuracy below that of standard VQE with a tight enough threshold. For the tight threshold of ϵ^{-4} both USCC and ADAPT-VQE have similar accuracies, except for at large bond stretching distances. Both USCC and ADAPT-VQE are able to produce errors smaller than standard VQE because both algorithms use different excitation schemes to generate the operator pool that selects the operators added to the ansatz. As described in an earlier section, USCC utilized disconnected triple and quadruple excitations in addition to the connected single and double excitations utilized in standard VQE. The larger excitation schemes allow USCC to capture more correlation energy that can only be captured by higher order excitations. This comes at the cost of an increase in the number of parameters, sometimes well above that of standard VQE. ADAPT-VQE generates a larger number of excitations by utilizing the generalized CCSD ansatz as described in a previous section. This excitation scheme does not distinguish between occupied and virtual orbitals when constructing excitation operators allowing for the potential of higher order excitations to be included.

Table 1 shows the average number of parameters required for non-symmetric H_2O at each threshold value for USCC and ADAPT-VQE compared to standard VQE. The number of parameters for the other molecules is given the the SI. While ADAPT-VQE and USCC can generate similar errors compared to FCI for similar thresholds, the number

Figure 5: ADAPT-VQE, USCC, and UCCSD-VQE energy differences from FCI plotted on a log scale for increasing interatomic distances with thresholds values of ϵ^{-1} , ϵ^{-2} , ϵ^{-3} , and ϵ^{-4} . The molecules tested are A. H_2 , B. LiH , C. non-symmetric H_6 , D. non-symmetric H_2O , and E. non-symmetric BeH_2 . The minimal STO-3G basis set was used for each calculation



of parameters required to achieve that accuracy are quite different. In order to match ADAPT-VQE's accuracy with threshold values of ϵ^{-4} , USCC requires over 2.6X the number of parameters. Similar trends occur for other molecules: 2.7X for LiH and non-

symmetric H_6 , and 3.4X for BeH_2 .

Table 1: Average number of parameters for ADAPT-VQE, USCC, and standard VQE at different threshold values for non-symmetric H_2O with the STO-3G basis set.

Method	H_4 (STO-3G)	H_4 (6-31G)	H_2O (STO-3G)
VQE	26	198	140
ADAPT-VQE (ϵ^{-1})	5	26	10
ADAPT-VQE (ϵ^{-2})	9	48	25
ADAPT-VQE (ϵ^{-3})	10	76	50
ADAPT-VQE (ϵ^{-4})	11	107	75
USCC (ϵ^{-1})	4	7	8
USCC (ϵ^{-2})	14	74	32
USCC (ϵ^{-3})	19	254	123
USCC (ϵ^{-4})	19	392	199

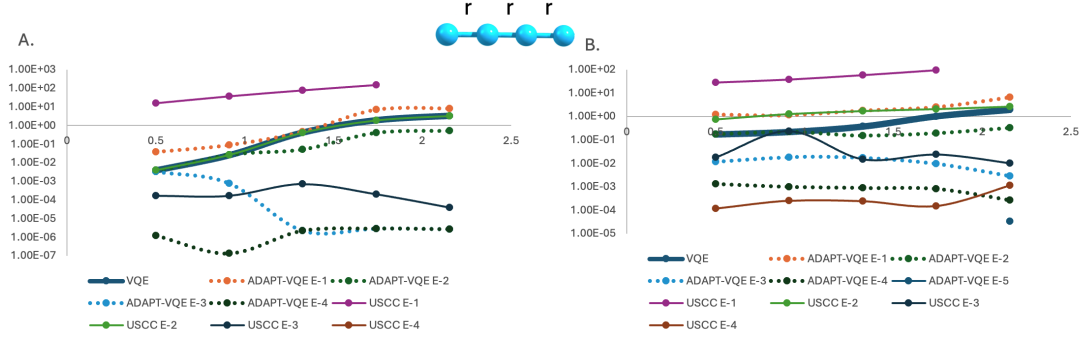
To test the effect of different basis sets on the flavors of VQE, calculations were run on a symmetric H_4 with both the minimal STO-3G basis set and the 6-31G Pople basis set. The difference in errors for each flavor of VQE shown in Figure 6 highlights the basis set dependence of each method. The reported energy differences are calculated with respect to the FCI energy at the given basis set. For all threshold values for both USCC and ADAPT-VQE, with the exception of USCC with ϵ^{-4} , the error between the VQE and FCI energy was larger for the 6-31G basis set compared to the error from the STO-3G basis set. The number of parameters required by USCC to match the accuracy of ADAPT-VQE with ϵ^{-4} also increases with larger basis sets with 1.7X and 3.7X parameters required by USCC for the STO-3GT and 6-31G basis sets respectively. Further, there are larger error differentiations between the different ϵ values. This is highlighted most clearly by the overlapping of the error points with the STO-3G basis set for USCC and ADAPT-VQE for the threshold values ϵ^{-3} and ϵ^{-4} that are more clearly separated in the 6-31G basis set errors. The changes in absolute errors and the distinctions introduced between threshold values are due to the increase in the number of available excitations from a larger number of virtual orbitals in the larger basis set. Larger basis sets do not expand the number of occupied orbitals, but expand the space of virtual orbitals available to the calculation. With

a larger number of virtual orbitals, the number of possible excitations in the operator pool increases for both ADAPT-VQE and USCC. With the minimal basis set, the possible number of operators for a small molecule is limited leading to a smaller set of operators with large gradient contributions. This means that a lower threshold value may not be able to capture any more meaningful correlation energy which leads to the aforementioned lack of distinction between the threshold values. When utilizing a larger basis set, which generates a larger operator pool, the number of operators that have small contributions to the correlation energy increase. With the increase in the number of operators with small gradient contributions, larger distinctions arise between different threshold values. The increase in the number of operators with smaller gradient contributions creates the basis set dependence of these effective Hamiltonian methods. As the basis set size increases the FCI energy gets closer to the exact energy (i.e. complete basis set extrapolation). This is due to the large increase in the number of small contributions from the enlarged virtual orbital space. As this virtual orbital space increases (and therefore the VQE operator pools increases), the cutoff thresholds capture a smaller percentage of these low lying contributions to the correlation energy. This leads to lower accuracy of the VQE methods with respect to the FCI energy as the basis set size increases. Therefore, as basis set size increases the cutoff threshold values must also be changed to capture an equivalent amount of information as compared to FCI.

6 Overview of different simulators and qubit mapping software

Quantum computing software ecosystems encompass quantum circuit simulators and qubit mapping (routing) tools. Simulators allow developers to run and debug quantum circuits on classical hardware, which is crucial in the NISQ era when real quantum processors are limited and noisy. As for qubit mapping tools, which are often part of compilers,

Figure 6: ADAPT-VQE, USCC, and UCCSD-VQE energy differences from FCI plotted on a log scale for increasing interatomic distances for symmetric H_4 on both A. the minimal basis set STO-3G and B. a larger basis set 6-31G to highlight any basis set dependence. As before the thresholds values were set to ϵ^{-1} , ϵ^{-2} , ϵ^{-3} , and ϵ^{-4} . Each collection of results with a given basis set is compared to the FCI energy calculated with that same basis set. The USCC ϵ^{-3} , and ϵ^{-4} data points for A. are overlapping and only show the one line trend.



they are responsible for translating an abstract quantum circuit into one that respects a specific hardware’s constraints (e.g., limited qubit connectivity).

Modern quantum simulators range from Software Development Kits (SDKs) integrated with cloud quantum hardware to specialized high-performance libraries. Key differences between simulators include open-source vs. proprietary licenses, support for CPU multi-threading or GPU acceleration, maximum feasible circuit size (qubit count), and integration with compilation or quantum hardware access. Below we discuss major frameworks and libraries:

6.1 Qiskit

Qiskit is IBM’s full-stack open-source SDK for quantum computing.⁵³ It includes the Aer simulator backend, which is highly flexible and efficient. Aer can simulate circuits using multiple methods: state-vector, density matrix, stabilizer (Clifford), and even tensor network approaches, automatically choosing the best method per circuit. It supports GPU acceleration via NVIDIA CUDA and offers a special GPU-enabled package (qiskit-aer-

gpu). Qiskit’s GPU state vector simulator was found to be the fastest for circuits up to about 16 qubits in a recent quantum volume benchmark.⁵⁴ Aer also supports multithreading and even MPI-based multi-node simulations for large problems. Integration-wise, Qiskit tightly integrates with IBM Quantum devices, allowing users to design circuits, simulate them, transpile, and then run on IBM’s real superconducting qubits with one framework. Qiskit is open-source and has an active community. Its simulator is considered state-of-the-art in performance, especially when combined with NVIDIA’s cuQuantum library⁵⁵ for additional speedups. One trade-off is that Qiskit-Aer’s GPU support is currently limited to NVIDIA GPUs. Overall, Qiskit Aer is a versatile, well-supported simulator with broad hardware integration and excellent performance on high-end systems.

6.2 Cirq and qsim

Cirq is an open-source Python framework from Google for designing and executing quantum circuits,^{56,57} especially tailored to NISQ experiments. Cirq represents circuits as moments of operations and has simple simulators included for state-vectors and density matrices (useful for small-scale tests and noisy simulations). For higher performance, Google provides qsim, a C++ simulation engine integrated with Cirq. Qsim is a full wave function (state vector) simulator that uses multithreading and gate fusion optimizations for speed. It is essentially an extension to Cirq, i.e. one writes circuits in Cirq and execute them via qsim for faster results. Qsim supports GPU-based simulations through its native CUDA backend (good for state amplitude extraction but less efficient for measurement sampling), or the NVIDIA cuQuantum/cuStateVec backend (faster sampling). For multi-GPU support, one has to use cuQuantum Appliance, which runs in a Docker container and has a version of qsim modified by NVIDIA. In a quantum volume benchmarking, qsim was the fastest pure-CPU simulator for circuits exceeding 16 qubits among several tested frameworks.⁵⁴ Cirq and qsim are Apache-licensed and integrate with Google’s

quantum processors. The Cirq framework’s design emphasizes direct control over low-level details such as qubit placements on a specific hardware grid, which is great for research but can make it slightly lower-level than Qiskit.

6.3 QuEST (Quantum Exact Simulation Toolkit)

QuEST is an open-source C library for high-performance computing (HPC) simulation.⁵⁸ According to its authors, QuEST is the “first open source, hybrid multithreaded and distributed, GPU-accelerated simulator of universal quantum circuits”. It can run on a single laptop or scale-up to supercomputers with thousands of nodes. QuEST supports both state-vectors and density matrices, and can utilize MPI for distributing a simulation across nodes. For example, using 2048 nodes QuEST authors simulated up to 38 qubits with full state-vectors.⁵⁸ It also supports GPUs within nodes (OpenMP + CUDA). In practice, QuEST is used in research that needs large quantum circuit simulations due to its excellent scaling on HPC systems. However, QuEST is a lower-level library: one writes C/C++ (or Python via wrappers), which is more involved than using Qiskit or Cirq. However, for sheer capability, QuEST is a top choice when maximum qubit count or performance is needed on clusters.

6.4 Qulacs

Qulacs is another fast C++ simulator with Python bindings.⁵⁹ It is optimized for single-node performance, using multi-threading and optional GPU acceleration. In CPU-only execution, Qulacs was found to be the fastest simulators for up 16 qubits in recent benchmarks.⁵⁴ This same benchmark showed that Qulacs on GPU performance was on par Qiskit GPU for large circuits. In fact, the Qulacs team introduced circuit optimizations that often make it outperform other simulators on typical gate benchmarks. Qulacs allows switching between a CPU backend and a GPU backend via a separate qulacs-gpu package with minimal code changes. It also supports an MPI extension (mpiQulacs) for

multi-node use, though with some limitations on available simulation methods. Qulacs is open source and has become a popular choice in academia for research that needs a fast simulator.

6.5 Intel Quantum SDK

Intel released an open-source SDK in 2023 that includes a compiler, runtime, and simulators.⁶⁰ The Intel Quantum Simulator is a state-vector simulator optimized for Intel CPUs and parallelization. It supports MPI for multi-node usage and can include noise models. In tests, the Intel simulator performed well especially at larger qubit counts (32+), where it was among the few to reach 33 qubits simulated.⁵⁴ Intel's SDK is a full stack and it even provides a C++ language extension to write “quantum kernels”. However, currently it only targets simulation since Intel doesn't have a cloud quantum hardware offering yet. This tool is mainly of interest to HPC users on Intel machines and those who want to experiment with Intel's proposed programming patterns.

6.6 Others

There are numerous other simulators such as Yao,⁶¹ JKQ DDSIM,⁶² AWS Braket simulators,⁶³ Qrack,⁶⁴ and Qibo⁶⁵ to name a few. In addition, more specialized simulators can be advantageous for certain use cases; for example, tensor network simulators can reach 50-100 qubits in circuits with limited depth or entanglement by contracting the circuit's tensor network rather than maintaining the full state vector.⁶⁶ These specialized methods, however, are beyond the scope of general-purpose software comparison since they often target specific circuit structures.

Overall, the quantum simulation landscape is predominantly defined by open-source software, spanning from comprehensive frameworks like Qiskit and Cirq to specialized HPC solvers such as QuEST and Qulacs. Modern simulators universally employ multi-core CPU parallelism, while state-of-the-art implementations frequently leverage NVIDIA

CUDA for GPU acceleration and distributed multi-node architectures to mitigate memory bottlenecks. Ultimately, simulator selection is driven by the specific research objective: frameworks like Qiskit and Cirq are preferred for their extensive SDKs and hardware connectivity, whereas lightweight solvers like Qulacs and QuEST are optimized for maximizing throughput on large-scale quantum circuits.

Recent development efforts in quantum simulation are divided between pushing the boundaries of exact simulation and enabling realistic NISQ emulation. A major focus is on scalability through approximation, utilizing tensor network methods like Matrix Product States to simulate significantly larger qubit counts for low-entanglement circuits, effectively bypassing the exponential memory cost of state vectors.⁶⁷ Concurrently, circuit knitting techniques are being integrated into SDKs, allowing users to decompose large circuits into smaller sub-circuits executable on smaller devices (or simulators), reconstructing the global result via classical post-processing.^{68,69}

Another axis of innovation lies in the rigorous modeling of decoherence, a defining challenge of the NISQ era. The focus has shifted from merely modeling ideal error channels to implementing sophisticated quantum error mitigation strategies directly within the simulation stack. Frameworks like Mitiq⁷⁰ and libraries within Qiskit now allow researchers to simulate and benchmark techniques such as zero-noise extrapolation⁷¹ and probabilistic error cancellation.⁷² These efforts aim not just to replicate hardware noise (often using data-driven noise profiles or digital twins of actual QPUs⁷³) but to actively suppress it, bridging the gap between raw hardware output and logical algorithm performance.

7 Conclusions and Outlook

The VQE method has been developed as an methodological response to the issues with the near term NISQ quantum computers computers. While methods like QPE show

promise for fault-tolerance quantum computers, the current hardware cannot support these calculations. Even the standard UCCSD-VQE method is insufficient for growing system sizes since the number of qubits requires scales with the growing number of operators. These increasingly large number of operators require more complex quantum circuit construction that can lead to high error rates on noisy quantum computers. As a response to the shortcoming of standard VQE, different flavors of VQE have been derived and implemented to create a more compact ansatz that requires fewer operators and scales better with increasing system size. ADAPT-VQE is well known to be a powerful algorithm for iteratively growing the ansatz to capture the bulk of the correlation energy while minimizing the number of parameters. In addition to the decrease in required parameters, ADAPT-VQE is shown to produce more accurate energies, with the lower number of parameters, when compared to standard VQE and other complexity reduction VQE methods. Benchmarking results show that as a general recommendation for ADAPT-VQE with the STO-3G basis set, a threshold value of ϵ^{-2} will generate errors below chemical accuracy and ϵ^{-3} will produce more accurate results than standard VQE. These guidelines are only suggested at the minimal STO-3G basis set, since the accuracy of these methods is shown to be basis set dependent.

While there are many current areas of research focused on further modifications to ADAPT-VQE that try to further decrease the number of parameters, generate more efficient gradients, and better map the operators to qubit space, there seems to be less interest in further modifying the generation of the operator pool to drive higher accuracy from ADAPT-VQE. It is shown that the generalized UCCSD ansatz produces an operator pool that better captures correlation energy with fewer number of parameters, but further development should focus on how to further optimize the accuracy of these methods while not greatly increasing the required number of parameters. Further work could be focused on increasing the accuracy of VQE methods by working to capture both dynamical and non-dynamical correlation. While the UCCSD based VQE method captures dynamical

correlation and methods like ADAPT-VQE-SCF work to capture non-dynamical correlation, the lack of orbital optimization in conjunction with the VQE method leaves important information out of the results. Classically intractable methods like multi-reference coupled cluster (MR-CC) or complete active space coupled cluster (CAS-CC) could exploit quantum algorithms to allow the iterative optimization of both dynamical and non-dynamical correlation to produce highly accurate results on complex systems.

8 Acknowledgment

This work was supported by the U.S. Department of Energy, Office of Science, Office of Basic Energy Sciences, Division of Chemical Sciences, Geosciences, and Biosciences at Argonne National Laboratory under contract no. DE-AC02-06CH11357. The authors gratefully acknowledge the computing resources provided on Improv, a high-performance computing cluster operated by the Laboratory Computing Resource Center at Argonne National Laboratory.

9 Author Contributions

T.H. and C.L. conceived the presented idea and analyzed the calculations. T.H. wrote and directed the manuscript, and ran benchmarking calculations. R.K. wrote the excited state method section. V.F.G. wrote the quantum simulator section. C.L. managed the project.

References

- (1) Feynman, R. P. Simulating Physics with Computers. *International Journal of Theoretical Physics* **1982**, *21*, 467–488.
- (2) Preskill, J. Quantum Computing in the NISQ Era and Beyond. *Quantum* **2018**, *2*, 79.
- (3) Choi, S.; Jarmolajev, I.; Huh, J. Variational Quantum Eigensolver with Fewer Qubits. **2020**,
- (4) Elfving, V. E.; Broer, B. W.; Webber, M.; Gavartin, J.; Halls, M. D.; Lorton, K. P.; Bochevarov, A. How Will Quantum Computers Provide an Industrially Relevant Computational Advantage in Quantum Chemistry? **2020**,
- (5) Kitaev, A. Y. Quantum measurements and the Abelian Stabilizer Problem. 1995; <https://arxiv.org/abs/quant-ph/9511026>.
- (6) Abrams, D. S.; Lloyd, S. Quantum Algorithm Providing Exponential Speed Increase for Finding Eigenvalues and Eigenvectors. *Physical Review Letters* **1999**, *83*, 5162–5165.
- (7) Nielsen, M. A.; Chuang, I. L. *Quantum Computation and Quantum Information*; Cambridge University Press, 2010.
- (8) Reiher, M.; Wiebe, N.; Svore, K. M.; Wecker, D.; Troyer, M. Elucidating reaction mechanisms on quantum computers. *Proceedings of the National Academy of Sciences* **2017**, *114*, 7555–7560.
- (9) Aharonov, D.; Ben-Or, M. Fault Tolerant Quantum Computation with Constant Error. **1996**,
- (10) Dobšíček, M.; Johansson, G.; Shumeiko, V.; Wendin, G. Arbitrary Accuracy Iterative Quantum Phase Estimation Algorithm Using a Single Qubit. *Physical Review A* **2007**, *76*, 030306.

(11) Wang, D.; Higgott, O.; Brierley, S. Accelerated Variational Quantum Eigensolver. *Physical Review Letters* **2019**, *122*, 140504.

(12) Kanno, K.; Kohda, M.; Imai, R.; Koh, S.; Mitarai, K.; Mizukami, W.; Nakagawa, Y. O. Quantum-Selected Configuration Interaction: classical diagonalization of Hamiltonians in subspaces selected by quantum computers. 2023; <https://arxiv.org/abs/2302.11320>.

(13) Peruzzo, A.; McClean, J.; Shadbolt, P.; Yung, M.-H.; Zhou, X.-Q.; Love, P. J.; Aspuru-Guzik, A.; O'Brien, J. L. A Variational Eigenvalue Solver on a Photonic Quantum Processor. *Nature Communications* **2014**, *5*, 4213.

(14) Jordan, P.; Wigner, E. Über das Paulische Äquivalenzverbot. *Zeitschrift für Physik* **1928**, *47*, 631–651.

(15) Reinholdt, P.; Ziems, K. M.; Kjellgren, E. R.; Coriani, S.; Sauer, S. P. A.; Kongsted, J. Critical Limitations in Quantum-Selected Configuration Interaction Methods. *Journal of Chemical Theory and Computation* **2025**, *21*, 6811–6822, PMID: 40586729.

(16) Nakagawa, Y. O.; Kamoshita, M.; Mizukami, W.; Sudo, S.; Ohnishi, Y.-y. ADAPT-QSCI: Adaptive Construction of an Input State for Quantum-Selected Configuration Interaction. *Journal of Chemical Theory and Computation* **2024**, *20*, 10817–10825.

(17) McClean, J. R.; Babbush, R.; Love, P. J.; Aspuru-Guzik, A. Exploiting Locality in Quantum Computation for Quantum Chemistry. *The Journal of Physical Chemistry Letters* **2014**, *5*, 4368–4380.

(18) Fedorov, D. A.; Alexeev, Y.; Gray, S. K.; Otten, M. J. Unitary Selective Coupled-Cluster Method. *Quantum* **2022**, *6*, 703.

(19) Bravyi, S.; Gambetta, J. M.; Mezzacapo, A.; Temme, K. Tapering off qubits to simulate fermionic Hamiltonians. 2017; <https://arxiv.org/abs/1701.08213>.

(20) Bravyi, S. B.; Kitaev, A. Y. Fermionic Quantum Computation. *Annals of Physics* **2002**, 298, 210–226.

(21) Grimsley, H. R.; Economou, S. E.; Barnes, E.; Mayhall, N. J. An Adaptive Variational Algorithm for Exact Molecular Simulations on a Quantum Computer. *Nature Communications* **2019**, 10, 3007.

(22) Tang, H. L.; Shkolnikov, V. O.; Barron, G. S.; Grimsley, H. R.; Mayhall, N. J.; Barnes, E.; Economou, S. E. Qubit-ADAPT-VQE: An Adaptive Algorithm for Constructing Hardware-Efficient Ansätze on a Quantum Processor. *PRX Quantum* **2021**, 2, 020310.

(23) Fitzpatrick, A.; Nykänen, A.; Talarico, N. W.; Lunghi, A.; Maniscalco, S.; García-Pérez, G.; Knecht, S. Self-Consistent Field Approach for the Variational Quantum Eigensolver: Orbital Optimization Goes Adaptive. *The Journal of Physical Chemistry A* **2024**, 128, 2843–2856.

(24) Yordanov, Y. S.; Arvidsson-Shukur, D. R. M.; Barnes, C. H. W. Efficient Quantum Circuits for Quantum Computational Chemistry. *Physical Review A* **2021**, 103, 032610.

(25) Benfenati, F.; Mazzola, G.; Capecci, C.; Barkoutsos, P. K.; Ollitrault, P. J.; Tavernelli, I.; Guidoni, L. Improved Accuracy on Noisy Devices by Non-Unitary Variational Quantum Eigensolver for Chemistry Applications. *arXiv preprint arXiv:2101.09316* **2021**,

(26) Tilly, J.; Chen, H.; Cao, S.; Picozzi, D.; Setia, K.; Li, Y.; Grant, E.; Wossnig, L.; Rungger, I.; Booth, G. H.; Tennyson, J. The Variational Quantum Eigensolver: A Review of Methods and Best Practices. *Physics Reports* **2022**, 986, 1–128.

(27) Wang, Q.; D'Cunha, R.; Mitra, A.; Alexeev, Y.; Gray, S. K.; Otten, M.; Gagliardi, L. Non-unitary Variational Quantum Eigensolver with the Localized Active Space Method and Cost Mitigation. 2025; <https://arxiv.org/abs/2501.13371>.

(28) Holmes, A. A.; Tubman, N. M.; Umrigar, C. J. Heat-Bath Configuration Interaction: An Efficient Selected Configuration Interaction Algorithm Inspired by Heat-Bath Sampling. *Journal of Chemical Theory and Computation* **2016**, *12*, 3674–3680.

(29) Westerheim, H.; Chen, J.; Holmes, Z.; Luo, I.; Nuradha, T.; Patel, D.; Rethinasamy, S.; Wang, K.; Wilde, M. M. Dual-VQE: A quantum algorithm to lower bound the ground-state energy. 2025; <https://arxiv.org/abs/2312.03083>.

(30) Feniou, C.; Hassan, M.; Traoré, D.; Giner, E.; Maday, Y.; Piquemal, J.-P. Overlap-ADAPT-VQE: practical quantum chemistry on quantum computers via overlap-guided compact Ansätze. *Communications Physics* **2023**, *6*.

(31) Feniou, C.; Hassan, M.; Claudon, B.; Courtat, A.; Adjoua, O.; Maday, Y.; Piquemal, J.-P. Greedy gradient-free adaptive variational quantum algorithms on a noisy intermediate scale quantum computer. *Scientific Reports* **2025**, *15*.

(32) Lan, Z.; Liang, W. Amplitude Reordering Accelerates the Adaptive Variational Quantum Eigensolver Algorithms. *Journal of Chemical Theory and Computation* **2022**, *18*, 5267–5275.

(33) Zhang, S.; Qin, Z.; Zhang, Y.; Zhou, Y.; Li, R.; Du, C.; Xiao, Z. Diffusion-Enhanced Optimization of Variational Quantum Eigensolver for General Hamiltonians. 2025; <https://arxiv.org/abs/2501.05666>.

(34) Shi, C.; Wang, H. Efficient Hamiltonian-aware Quantum Natural Gradient Descent for Variational Quantum Eigensolvers. 2025; <https://arxiv.org/abs/2511.14511>.

(35) Stenger, J. P. T.; Hellberg, C. S.; Gunlycke, D. Hybrid VQE-CVQE algorithm using diabatic state preparation. 2025; <https://arxiv.org/abs/2512.04801>.

(36) Zhang, Y.; Cincio, L.; Negre, C. F. A.; Czarnik, P.; Coles, P. J.; Anisimov, P. M.;

Mniszewski, S. M.; Tretiak, S.; Dub, P. A. Variational Quantum Eigensolver with Reduced Circuit Complexity. *npj Quantum Information* **2022**, *8*, 96.

(37) Rissler, J.; Noack, R. M.; White, S. R. Measuring orbital interaction using quantum information theory. *Chemical Physics* **2006**, *323*, 519–531.

(38) Ryabinkin, I. G.; Lang, R. A.; Genin, S. N.; Izmaylov, A. F. Iterative Qubit Coupled Cluster Approach with Efficient Screening of Generators. *Journal of Chemical Theory and Computation* **2020**, *16*, 1055–1063.

(39) Lim, H.; Kang, D. H.; Kim, J.; Pellow-Jarman, A.; McFarthing, S.; Pellow-Jarman, R.; Jeon, H.-N.; Oh, B.; Oh, S.; Rhee, J.-K. K.; No, K. T. Fragment Molecular Orbital-Based Variational Quantum Eigensolver for Quantum Chemistry in the Age of Quantum Computing. *Scientific Reports* **2024**, *14*, 2422.

(40) Barca, G. M. J. et al. Recent developments in the general atomic and molecular electronic structure system. *J. Chem. Phys.* **2020**, *152*, 154102.

(41) Nakano, T.; Kaminuma, T.; Sato, T.; Akiyama, Y.; Uebayasi, M.; Kitaura, K. Fragment molecular orbital method: application to molecular dynamics simulation of proteins. *Chem. Phys. Lett.* **2000**, *318*, 614–618.

(42) Roos, B. O.; Taylor, P. R.; Siegbahn, P. E. M. A Complete Active Space SCF Method (CASSCF) Using a Density Matrix Formulated Super-CI Approach. *Chemical Physics* **1980**, *48*, 157–173.

(43) Siegbahn, P. E. M.; Heiberg, A.; Roos, B. O.; Levy, B. A Comparison of the Super-CI and the Newton-Raphson Scheme in the Complete Active Space SCF Method. *Physica Scripta* **1981**, *21*, 323.

(44) Hermes, M. R.; Gagliardi, L. Multiconfigurational Self-Consistent Field Theory

with Density Matrix Embedding: The Localized Active Space Self-Consistent Field Method. *Journal of Chemical Theory and Computation* **2019**, *15*, 972–986.

(45) Tran, H. Q.; Hermes, M. R.; Gagliardi, L. Multiconfigurational Self-Consistent Field Theory with Density Matrix Embedding: The Localized Active Space Self-Consistent Field Method. *Journal of Chemical Theory and Computation* **2019**, *15*, 972–986.

(46) Higgott, O.; Wang, D.; Brierley, S. Variational Quantum Computation of Excited States. *Quantum* **2019**, *3*, 156.

(47) Gocho, S.; Nakamura, H.; Kanno, S.; Gao, Q.; Kobayashi, T.; Inagaki, T.; Hatanaka, M. Excited state calculations using variational quantum eigensolver with spin-restricted ansätze and automatically-adjusted constraints. *npj Computational Materials* **2023**, *9*, 13.

(48) Cadi Tazi, L.; Thom, A. J. Folded spectrum vqe: A quantum computing method for the calculation of molecular excited states. *Journal of Chemical Theory and Computation* **2024**, *20*, 2491–2504.

(49) Ollitrault, P. J.; Kandala, A.; Chen, C.-F.; Barkoutsos, P. K.; Mezzacapo, A.; Pistoia, M.; Sheldon, S.; Woerner, S.; Gambetta, J. M.; Tavernelli, I. Quantum equation of motion for computing molecular excitation energies on a noisy quantum processor. *Physical Review Research* **2020**, *2*, 043140.

(50) Pavosevic, F.; Hammes-Schiffer, S. Multicomponent unitary coupled cluster and equation-of-motion for quantum computation. *Journal of Chemical Theory and Computation* **2021**, *17*, 3252–3258.

(51) Asthana, A.; Kumar, A.; Abraham, V.; Grimsley, H.; Zhang, Y.; Cincio, L.; Tretiak, S.; Dub, P. A.; Economou, S. E.; Barnes, E.; others Quantum self-consistent equation-of-motion method for computing molecular excitation energies, ionization potentials, and electron affinities on a quantum computer. *Chemical Science* **2023**, *14*, 2405–2418.

(52) Jensen, P. W.; Kjellgren, E. R.; Reinholdt, P.; Ziems, K. M.; Coriani, S.; Kongsted, J.; Sauer, S. P. Quantum equation of motion with orbital optimization for computing molecular properties in near-term quantum computing. *Journal of Chemical Theory and Computation* **2024**, *20*, 3613–3625.

(53) Javadi-Abhari, A.; Treinish, M.; Krsulich, K.; Wood, C. J.; Lishman, J.; Gacon, J.; Martiel, S.; Nation, P. D.; Bishop, L. S.; Cross, A. W.; others Quantum computing with Qiskit. *arXiv preprint arXiv:2405.08810* **2024**,

(54) Boehme, C.; van Niekerk, L.; Kumar, D.; Sharma, A. K.; Meisel, T.; Paleico, M. L. A Comparison of HPC based Quantum Computing Simulators using Quantum Volume. *INFORMATIK* **2024**. 2024; pp 579–589.

(55) Bayraktar, H.; Charara, A.; Clark, D.; Cohen, S.; Costa, T.; Fang, Y.-L. L.; Gao, Y.; Guan, J.; Gunnels, J.; Haidar, A.; others cuquantum sdk: A high-performance library for accelerating quantum science. 2023 IEEE International Conference on Quantum Computing and Engineering (QCE). 2023; pp 1050–1061.

(56) Developers, C. *Cirq*; Zenodo, 2025.

(57) team, Q. A.; collaborators qsim. 2020; <https://doi.org/10.5281/zenodo.4023103>.

(58) Jones, T.; Brown, A.; Bush, I.; Benjamin, S. C. QuEST and high performance simulation of quantum computers. *Scientific reports* **2019**, *9*, 10736.

(59) Suzuki, Y.; Kawase, Y.; Masumura, Y.; Hiraga, Y.; Nakadai, M.; Chen, J.; Nakanishi, K. M.; Mitarai, K.; Imai, R.; Tamiya, S.; others Qulacs: a fast and versatile quantum circuit simulator for research purpose. *arXiv preprint arXiv:2011.13524* **2020**,

(60) Khalate, P.; Wu, X.-C.; Premaratne, S.; Hogaboam, J.; Holmes, A.; Schmitz, A.; Guerreschi, G. G.; Zou, X.; Matsuura, A. Y. An LLVM-based C++ compiler toolchain for

variational hybrid quantum-classical algorithms and quantum accelerators. *arXiv preprint arXiv:2202.11142* **2022**,

(61) Luo, X.-Z.; Liu, J.-G.; Zhang, P.; Wang, L. Yao. jl: Extensible, efficient framework for quantum algorithm design. *arXiv preprint arXiv:1912.10877* **2019**,

(62) Wille, R.; Hillmich, S.; Burgholzer, L. JKQ: JKU tools for quantum computing. Proceedings of the 39th International Conference on Computer-Aided Design. 2020; pp 1–5.

(63) Amazon Web Services Amazon Braket. 2020; <https://aws.amazon.com/braket/>.

(64) Strano, D.; Bollay, B.; Blaauw, A.; Shammah, N.; Zeng, W. J.; Mari, A. Exact and approximate simulation of large quantum circuits on a single GPU. 2023 IEEE International Conference on Quantum Computing and Engineering (QCE). 2023; pp 949–958.

(65) Efthymiou, S.; Ramos-Calderer, S.; Bravo-Prieto, C.; Pérez-Salinas, A.; García-Martín, D.; Garcia-Saez, A.; Latorre, J. I.; Carrazza, S. Qibo: a framework for quantum simulation with hardware acceleration. *Quantum Science and Technology* **2021**, *7*, 015018.

(66) Fried, E. S.; Sawaya, N. P.; Cao, Y.; Kivlichan, I. D.; Romero, J.; Aspuru-Guzik, A. qTorch: The quantum tensor contraction handler. *PloS one* **2018**, *13*, e0208510.

(67) García, M. D.; Romero, A. M. Survey on Computational Applications of Tensor Network Simulations. *IEEE Access* **2024**, *12*, 193212–193228.

(68) Piveteau, C.; Sutter, D. Circuit knitting with classical communication. *arXiv preprint arXiv:2205.00016* **2022**,

(69) Mitarai, K.; Fujii, K. Constructing a virtual two-qubit gate by sampling single-qubit operations. *New Journal of Physics* **2021**, *23*, 023021.

(70) LaRose, R.; Mari, A.; Kaiser, S.; Karalekas, P. J.; others Mitiq: A software package for error mitigation on noisy quantum computers. *Quantum* **2022**, *6*, 774.

(71) Li, Y.; Benjamin, S. C. Efficient variational quantum simulator incorporating active error minimisation. *Physical Review X* **2017**, *7*, 021050.

(72) Temme, K.; Bravyi, S.; Gambetta, J. M. Error mitigation for short-depth quantum circuits. *Physical Review Letters* **2017**, *119*, 180509.

(73) Muller, M.; Zanner, M.; others Towards a Digital Twin of Noisy Quantum Computers: Calibration-Driven Emulation of Transmon Qubits. *arXiv preprint arXiv:2504.08313* **2025**,